NUMERICAL SIMULATION OF ROCK RAMP FISHWAY FOR SMALL-BODIED GREAT PLAINS FISHES

by

Cindy Chidumebi Ufelle

A thesis submitted in partial fulfillment
of the requirements for the degree

of

Master of Science

in

Civil Engineering

MONTANA STATE UNIVERSITY
Bozeman, Montana

December 2023

©COPYRIGHT

by

Cindy Chidumebi Ufelle

2023

All Rights Reserved

DEDICATION

To my mom
For her love and support.

ACKNOWLEDGEMENTS

Undoubtedly, this work would not have been possible without the help, input, suggestions, encouragement, and collaboration of a number of people. Therefore;

First, I would like to convey my most profound appreciation and gratitude to my advising committee of Dr. Kathryn Plymesser, Dr. Joel Cahoon, and Dr. Matt Blank for their technical expertise, support, valuable guidance, constructive criticism, and encouragement given during every stage of this research. Special thanks to Dr. Chris Myrick and Tyler Swarr for their support and collaboration in this research. I would also like to thank Dr. Flynn Murray for always being there to support me academically and emotionally.

More thanks are due to my colleagues and office mates, Samanthi Wijerathna, Wyatt Alt, Sam Steele, Bishal Dhakal, Sam Curtis, and Chidimma Ifeh, for their continuous support throughout my study period. Your help was invaluable!

I am deeply grateful to all the faculty and staff of the Department of Civil Engineering, Montana State University, for their support.

Finally, I would like to thank my loving mother and siblings, without whom this venture would not have been possible. I am forever grateful for their patience, faith, support, and unconditional love for me, which gives me strength in every step I take.

TABLE OF CONTENTS

1. CHAPTER ONE: LITERATURE REVIEW 1

Introduction 1
Rock Ramp Fishway Passage Studies 5
Rock Ramp Fishway Hydraulics Studies 13
Physical Model Studies 14
CFD Model Studies 26
Great Plains Fish Species of Interest 33
Discussion 35

2. CHAPTER TWO: ROCK RAMP MODELING 37

Introduction 37
CFD Theory 40
Methods 46
Model Development and Design 46
Mesh Independence Study 55
Sensitivity Test 58
Turbulence model 58
Roughness 59
Model Validation 61
Velocity 62
Flow depth 65
Results and Discussion 69
Flow Depth 71
Velocity 73
Turbulent Kinetic Energy 82
Conclusion 86

REFERENCES CITED 88

LIST OF TABLES

Table Page

1. Table 2.1: Slopes and their respective flow rates used in the experimental study. 50
2. Table 2.2: Summary of the boundary conditions. 52
3. Table 2.3: Summary of the grid sizes. 56
4. Table 2.4: Summary of the results of the model validation measured along the centerline. 69
5. Table 2.5: Summary of the results of the model validation measured along the mid cross section. 69
6. Table 2.6: Summary of the predicted values for the flow depths. 70
7. Table 2.7: Summary of the predicted values for the flow velocities. 70
8. Table 2.8: Summary of the predicted values for the turbulence kinetic energy. 70

LIST OF FIGURES

Figure Page

1. Figure 2.1: The flume and fishway geometry dimensions. 46
2. Figure 2.2: The rock being scanned with the Artec Space Spider 3D Scanner. 47
3. Figure 2.3: The fishway (left) and rock (right) 3-D STL geometries. 48
4. Figure 2.4: The three mesh blocks used for the fishway (left) and the conforming mesh (right). 49
5. Figure 2.5: The boundary conditions for the three mesh blocks. 51
6. Figure 2.6: The RMSE plot for the different mesh sizes. 57
7. Figure 2.7: Plot of the free surface elevation along the longitudinal centerline for the turbulence models. 59
8. Figure 2.8: Plot of the free surface elevation along the longitudinal centerline for the roughness heights. 60
9. Figure 2.9: Velocities comparison between the simulated and the measured values at the 2% and 10% slopes along the streamwise centerline. 63
10. Figure 2.10: Velocities comparison between the simulated and the measured values at the 2% and 10% slopes along the mid cross-section. 64
11. Figure 2.11: Water depth comparison between the simulated and the measured values at the 2% and 10% slopes along the streamwise centerline. 66
12. Figure 2.12: Water depth comparison between the simulated and the measured values at the 2% and 10% slopes along the mid cross-section. 67
13. Figure 2.13: The model domain visualized for flow depths. 72
14. Figure 2.14: Longitudinal flow depths for the different slopes colored by velocity. 73
15. Figure 2.15: Plan view of the fishway illustrating the velocity for the different slopes 74
16. Figure 2.16: Upstream distance covered by the fish species for different slopes for passage probabilities greater than 20% (Swarr, 2018). 76

LIST OF FIGURES CONTINUED

Figure Page

17. Figure 2.17: Visualized Cross-sections for the velocities between and behind the two-rock and three-rock rows. 77

18. Figure 2.18: Cross-sectional velocity between two rocks. 78

19. Figure 2.19: Cross-sectional velocity between three rocks. 79

20. Figure 2.20: Cross-sectional velocity behind two rocks. 80

21. Figure 2.21: Cross-sectional velocity behind three rocks. 81

22. Figure 2.22: Plan view of the fishway illustrating the Turbulent Kinetic Energy for the different slopes. 84

23. Figure 2.23: Longitudinal view of the Turbulent Kinetic Energy for the different slopes..... 85

24. Figure 2.24: Longitudinal view of the velocity vectors for the different slopes..... 85

ABSTRACT

The preservation and restoration of fish populations and their habitats have become significant aspects of environmental conservation efforts. Effectiveness of fish passage structures plays a crucial role in facilitating the successful migration of various fish species. This research focused on utilizing Computational Fluid Dynamics (CFD) models to assess the hydraulic conditions within a rock ramp fishway with varying slopes and flow rates for small-bodied Great Plains fishes. This work built upon a previous study conducted by Swarr (2018) to investigate the passage success rates of three small-bodied fish of the Great Plains of North America: Flathead Chub (*Platygobio gracilis*), Arkansas Darter (*Etheostoma cragini*), and Stonecat (*Noturus flavus*) within a full-scale laboratory rock ramp fishway. Using commercial software, Flow-3D Hydro, CFD models were developed to simulate and predict hydraulic parameters such as flow depths, velocities, and turbulence kinetic energies (TKEs) within the fishway. To validate the accuracy of the CFD models, predicted flow depths and velocities were compared with observed data for two slopes: 2% and 10%. The CFD model results indicated that increasing slopes and flow rates led to corresponding increases in the mean values of the studied parameters. The mean depth varied from 0.051 m on the 2% slope to 0.068 m on the 10% slope. The mean velocity increased from 0.272 m/s on the mildest slope to 1.003 m/s on the steepest slope. Additionally, the average TKE ranged from 0.003 J/kg on the 2% slope to 0.014 J/kg on the 10% slope. The study highlighted that higher velocity and TKE values at steeper slopes may have contributed to the poor upstream passage rate, particularly for weaker swimmer species, like the Arkansas Darter, at slopes greater than 4%, as observed in the physical model study. Findings demonstrated that the presence of rocks in the fishway created diverse flow conditions. Low-velocity zones observed behind rocks within the fishway may provide favorable conditions for successful fish ascent. This research showcases the capabilities of CFD in providing quantitative data for optimizing fish passage structure design and contributing to conservation efforts.

CHAPTER ONE: LITERATURE REVIEW

Introduction

As the world changes due to modernization, humans have found ways to control and manipulate water for various purposes. Instream modifications such as dams, culverts, and other hydraulic structures have been designed and built across rivers and streams worldwide. Dams were constructed to store or divert water for human consumption and livestock, irrigation, flood control, power generation, recreational activities, and other purposes. The United States Army Corps of Engineers (USACE) has documented the existence of over 90,000 dams within the United States of America (USA) through its National Inventory of Dams (NID) database. Although dams have benefited humans, there are some drawbacks, including river system fragmentation, destruction of natural habitats, ecological hazards, and displacement of people (Zhang et al., 2018). Most fish species depend on the longitudinal connectivity of the river to access habitats for reproduction, growth, and survival.

Stream fragmentation has significant implications for migratory fishes. Species richness, population abundance, and assemblage structure can be impacted by river fragmentation (Cooper et al., 2017). Changes to the environment, both direct and indirect, can have a negative impact on fish populations, potentially leading to extinction (Cooper, 2013). Local extinctions of small-bodied fishes have been attributed to stream fragmentation in North America, Asia, Europe, and Australia (Ficke et al., 2011).

In the Great Plains of North America, stream fragmentation is primarily due to the construction of instream barriers, which has impacted stream connectivity (Perkin et al., 2015; Swarr, 2018). Dams in the Great Plains have caused population decline as they prevent the

upstream migration of fish. This is particularly true for small-bodied fishes endemic to the Great Plains, such as the pelagic spawning minnows, impacting their population and causing declines (Pennock et al., 2018). Additionally, stream fragmentation in the rivers of the Great Plains has created conditions conducive to the proliferation of non-native species. As barriers prevent the movement of native species, invasive species that are better adapted to altered conditions might gain a competitive advantage. For instance, larger, invasive species such as Smallmouth Bass (*Micropterus dolomieu*) can outcompete small-bodied native fishes for food and habitat (Kirk et al., 2022). This results in the displacement and extirpation of native species. In addition, this further disrupts the natural balance of fish communities and leads to their growing homogenization (Perkin et al., 2015; Pennock, 2016).

To re-establish wildlife connectivity in fragmented streams, dam removal may be the best approach. Removing dams can enhance connectivity by reconnecting fragmented habitats, thereby restoring the stream to its natural state. However, due to the benefits of dams and economic challenges, removing dams is not always feasible (Raabe et al., 2019). In these cases, fish passages (also known as fishways) can be a suitable alternative. Fishways are incorporated into the design of hydraulic structures or are retrofitted to existing dams (Ficke et al., 2011; Stoller et al., 2016). Fishways are hydraulic structures that enable fish to navigate barriers as they move upstream and are categorized into two groups, technical and nature-like fishways (NLFs) (Cassan & Laurens, 2016; Richer et al., 2020; Rice, 2021).

Technical fishways are built from engineered materials, such as wood, metal, fiberglass, or concrete, to produce stepped channels with flat surfaces (Stoller et al., 2016). These stepped channels are divided by weirs, baffles, walls, chutes, and vanes (Katopodis et al., 2001).

Technical fishway types include pool and weir, Denil, vertical slot, Alaska steeppass, and fish locks (Rice, 2021).

Nature-like fishways are built with natural materials such as rocks, gravel, boulders, riparian vegetation, and wood to mimic the geomorphological conditions of natural stream channels (Bretón et al., 2013; Zheng et al., 2020). They have gained recognition as an environmentally friendly alternative to technical fishways (Baki & Azimi, 2021). Flow conditions within a cross-section of NLFs are diverse. This makes them accessible to many fish species, including small-bodied fishes (Katopodis & Williams, 2012). Nature-like fishways can be further subdivided into nature-like bypass channels and rock ramps (Cassan & Laurens, 2016; Richer et al., 2020). Bypass channels are constructed as side channels that flow around dam structures. Rock ramps are constructed inside stream channels, going up to and over pre-existing dams. Ramps span the entire width of the stream (Stoller et al., 2016). Most of the time, NLFs, including the nature-like bypass channel, are referred to as rock ramp fishways (Swarr, 2018). Unlike technical fishways, there is still a gap in knowledge regarding the understanding of hydraulic conditions and successful passage for target species in NLFs (Raabe et al., 2019; Richer et al., 2020). This gap needs to be filled to increase understanding of the NLFs for best practices to conserve Great Plains small-bodied fish that are affected by fragmentation. Rock ramp fishways generally consist of a long sloping channel with scattered but closely spaced immobile rocks or boulders. These rocks are arranged in such a way that they reduce the flow velocity, increase water depth, and dissipate energy. Rock ramp fishways also reduce the likelihood of clogging due to adequate spacing between boulders for debris to pass and the boulders provide resting places for fish as they move upstream (Baki et al., 2017a; Miranda et

al., 2021). Rock ramp fish passes are not only functional and maintainable but also aesthetically pleasing (Steffensen et al., 2013; Raabe et al., 2019). They are typically wide channels with a low gradient (< 5% slope) (Haro et al., 2008), to imitate the natural river gradient, and are becoming a popular option for fish passage, particularly at low-head dams (Steffensen et al., 2013).

Researchers have been studying the performance of rock ramp fishways in restoring longitudinal connectivity. Some of these studies have explored attraction and passage efficiency using models conducted in real-world field conditions, allowing for a more accurate representation of natural environments. Others have utilized laboratory models that allow for variable manipulations and specific effects observation. These models are created by constructing the rock ramp fishway and installing it in an indoor channel or flume. While laboratory models offer controlled conditions conducive to study, findings from such studies might not always reflect the complexities of field environments. Hydraulic studies of rock ramp fishways were mostly conducted using laboratory models. In recent years, the use of numerical approaches, especially computational fluid dynamics (CFD) models, in conducting hydraulic studies in fishways and habitat structures has increased greatly. Plymesser (2014) used Flow 3D software to model a technical fishway. The commercial software, STAR-CCM+, was used by Juras et al. (2018) for a habitat structure study. Baki et al. (2016), Baki et al. (2017a), Baki et al. (2017b), and Baki et al. (2020) used the ANSYS-CFX software to investigate the flow characteristics within a rock ramp fish passage. Chorda et al. (2019) and Miranda et al. (2021) used OpenFOAM software in their nature-like fishway studies. Complementing fish passage

studies with CFD modeling will provide a more comprehensive understanding of fishway hydraulics.

Rock Ramp Fishway Passage Studies

Studies of fish passage within rock ramp fishways have gained significant attention in recent years. These studies aim to provide valuable insights into the design and operation of rock ramp fishways by evaluating fish species behavior, movement patterns, and passage success rates. The goal is to optimize the functionality of these rock ramp fishways and maximize their potential for conserving and restoring fish populations.

Franklin et al. (2012) investigated passage success of anadromous adult Alewives (Alosa pseudoharengus) across multiple fishway designs. Their study encompassed the evaluation of two rock ramp fishways, two technical steeppass fishways, and one technical pool-and-weir fishway at Town Brook in Plymouth, Massachusetts and East River in Guilford, Connecticut, USA. The rock ramp fishway in Town Brook is 8 m wide, 32 m long, and set on a slope of 4.2%, while the rock ramp fishway in East River is in a bypass, covering a length of 48 m, and has a slope of 7.1%. Passive integrated transponder (PIT) telemetry was used to quantify the upstream movements of adult Alewives. The findings of their study revealed a high success rate associated with passage of Alewives through the rock ramp fishway at Town Brook. In the analysis of the Town Brook fishway, a passage success rate of 94% was observed among the 103 Alewives studied. Out of these, 97 Alewives successfully ascended the fishway, with 91 of them passing successfully on their first attempt. For the East River, 91.8% of the 231 fishes detected at the entrance of the bypass entered the rock ramp fishway. However, the passage success rate within the fishway was only 40%, indicating that a significant portion of the fish that entered did not

pass successfully. The low passage observed in the East River bypass was attributed to some combination of flow and temperature, with lower temperatures reducing passage performance (Franklin et al., 2012).

Steffensen et al. (2013) conducted an evaluation of a nature-like fishway installed on a low-head dam situated on Indian Creek in southeastern Ontario, Canada. The dam is 11.1 m wide and 1.45 m high. The primary objective was to assess the attraction and passage efficiency of a warm-water fish assemblage through the fishway during their spring spawning migration. The fishway is a rock ramp bypass fishway that is 116 m long with an average slope of 1.25%. PIT telemetry was used to evaluate fishway attraction and passage efficiency for seven fish species. However, the detailed analyses focused on the three most abundant species: Common Shiner (*Luxilus comutus*), White Sucker (*Catostomus commersonii*), and Creek Chub (*Semotilus atromaculatus*). The study utilized four pass-over antennas positioned within the fishway, and two pass-through antennas installed upstream and downstream of the fishway entrance. These pass-through antennas aimed to detect tagged fish moving upstream or downstream of the fishway entrance. The evaluation process involved comparing the number of tagged fish detected at the fishway entrance antenna with those detected at the two pass-through antennas to determine attraction efficiency. Furthermore, passage efficiency was calculated by comparing the proportion of fish that successfully ascended the fishway to those that entered the fishway. The authors noted that out of 391 tagged fishes, 149 were not detected by any of the antennas used in the study. Their analysis and evaluation showed attraction efficiencies were 63.3% for Common Shiner, 65.6% for White Sucker, and 83.7% for Creek Chub, while their passage efficiencies were 5.1%, 25%, and 38.4% respectively. To understand the reason for the low passage

efficiency, the researchers released some Creek Chub in the lower reaches of the fishway and observed an increase in passage efficiency to 76.2%. The authors deduced the water level within the fishway was too low for some of the fish to use. This study brought to light the importance of water depth for successful passage in rock ramp fishways (Steffensen et al., 2013).

Stoller et al. (2016) observed the effectiveness of a rock ramp fishway as a tool to restore stream connectivity. They compared the summer fish assemblage composition in a river with a rock ramp retrofitted to the Chesaning Dam (Shiawassee River) to a nearby river that is dammed (Cass River) and a nearby free-flowing river (Flint River) in the Lake Huron Basin in Michigan, USA. The authors quantified the performance of the fishway by analyzing the fish assemblage composition. To compare the upstream and downstream fish assemblages, they utilized three metrics: species richness, the proportion of total catch, and mean catch-per-unit-effort (CPUE). The study was conducted over two years, in 2011 and 2012. The results showed the rock ramp improved stream connectivity and had higher similarity to a free-flowing river in terms of species richness and proportional abundance. However, it did not completely restore passage across the Chesaning Dam for certain targeted families like Centrarchids and Percids. It was found that the dammed river exhibited the highest species richness. A total of 54 species were caught across all sites and years in this river. The rock-ramp river had the second highest species richness, with a total of 48 species observed. In contrast, the free-flowing river had the lowest species richness, with a total of 44 species identified (Stoller et al., 2016).

Dodd et al. (2017) explored the effectiveness of a nature-like bypass in restoring longitudinal connectivity for Brown Trout (*Salmo trutta L.*). The study was conducted on the River Aire in Yorkshire, England, and involved construction of a 150 m long nature-like bypass

channel with an average slope of 1.2% at Rodley Weir. The weir is 1.8 m high and 50 m wide. The attraction and passage efficiencies were quantified using a PIT tag system. The efficiency of the fishway was evaluated using four metrics: (1) Attraction efficiency was determined by calculating the percentage of tagged Brown Trout found at the entrance relative to the total number tagged; (2) Entrance efficiency measured the percentage of the fish found at the entrance that eventually entered the fishway; (3) Passage efficiency was the percentage of fish that entered the fishway and successfully exited at the upstream exit of the fishway; and (4) Exit efficiency was evaluated by considering the percentage of fish that reached the upstream exit without moving back downstream into the fishway. The data from the study indicated that out of 111 tagged Brown Trout, 57 were attracted to the downstream end of the fishway (attraction efficiency of 51%). Of the 57 fish that reached the fishway entrance, 49 subsequently entered (entrance efficiency of 89%). Thirty-eight of the 49 tagged fish that entered the fishway successfully ascended and exited at the upstream end (passage efficiency of 78%). All but one of the 38 fish that reached the fishway exit left without moving back downstream (exit efficiency of 97%). The authors observed larger fish were attracted to the fishway. This led them to propose the smaller tagged fish might consist of sub-adults who do not require migration for spawning purposes. This finding shed light on the potential role of the fishway in accommodating different life stages of fish. Furthermore, throughout the long duration of the study, fish were consistently detected within the fishway, regardless of flow conditions and time of day. This implies the fishway serves a dual purpose by facilitating fish migration while also providing a refuge for fish. Overall, this study provided compelling evidence supporting the effectiveness of the nature-like fishway in enhancing ecological conditions (Dodd et al., 2017).

Swarr (2018) conducted research aimed at enhancing the design of rock ramp fishways by determining the optimal combinations of slope and length for successful passage of small-bodied Great Plains fish species. The study was conducted using a prototype rock ramp fishway installed in a laboratory flume at the Colorado State University (CSU) Foothills Fisheries Laboratory. The experimental flume had dimensions of 9.1 m in length and 1.2 m in width, while the fishway itself was 6.1 m long with a trapezoidal cross-section featuring side slopes inclined at 30° and a central channel width of 0.61 m. The target fish species were Flathead Chub (*Platygobio gracilis*), Stonecat (*Noturus flavus*), and Arkansas Darter (*Etheostoma cragini*). These species were chosen based on their distinct swimming abilities and the availability of prior swimming performance data. The study involved testing success of fish passage through the experimental rock ramp fishway at various slopes, ranging from 2% to 10%. The fish species were assessed separately in groups of five (Stonecats) or ten (Flathead Chub and Arkansas Darters) individuals per trial. Transferred from their tanks to the fishway, the fish were given 20 hours to ascend the fishway. The movements of the fish were continuously monitored using the PIT tag technique, facilitated by four pass-over antennas positioned at intervals of 2.03 m within the fishway. The movement data collected were subjected to analysis utilizing the Cormack-Jolly-Seber (CJS) model, which enabled the determination of the probability of full or partial passage success. The insights derived from full and partial passage success data were instrumental in identifying the optimal combinations of length and slope for the design of future fishways. Additionally, the researchers employed Program MARK, a Windows-based software application, to calculate maximum likelihood estimates of movement probabilities. The results of the study indicated Flathead Chubs, known for their strong swimming abilities, achieved a 100%

probability of successfully navigating the entire 6.1 m of the fishway at slopes of 2%, 4%, and 6%. In contrast, Stonecats had a 100% passage success rate at the 2% and 4% slopes in ascending the full 6.1 m length of the rock ramp fishway, and 83% for a distance of 4.06 m at the 6% slope. Meanwhile, Arkansas Darters, characterized by limited swimming ability, did not attain a probability of 100% for ascending the full 6.1 m fishway. However, they displayed moderate probabilities of partially succeeding at lower slopes, with a 43% probability for covering an upstream distance of 2.03 m at the 4% slope and a 54% probability for a distance of 4.06 m at the 2% slope. Furthermore, the study identified that shorter fishway lengths, approximately 2 m at a 4% slope, resulted in the highest passage success for all three tested species. Longer lengths or steeper slopes were found to decrease passage success rates for these species. In conclusion, the study demonstrated that rock ramp fishways can effectively facilitate passage of various small-bodied fish species, including those with relatively poor swimming abilities. The researchers recommended designing fishways with shorter lengths and slopes up to 4% to maximize passage success for small-bodied and juvenile fishes (Swarr, 2018).

Murry et al. (2020) continued to evaluate the effectiveness of the rock ramp fishway studied by Stoller et al. (2016). Their research focused on evaluating the impact of a rock ramp fish passage on fish migration in the Shiawassee River, a tributary of Saginaw Bay in Lake Huron, Michigan, USA, with a particular emphasis on fish species during their spring migratory runs. The researchers compared the fish assemblage between the rock ramp fishway and the dammed river (Cass River). To gauge the efficacy of this fishway, the researchers employed various methods, including non-metric multi-dimensional scaling (NMDS), multi-response permutation procedure (MRPP), egg-collecting techniques, and fish mark-recapture.

Additionally, boat electrofishing was utilized to assess fish species abundance in different sections of the river during the spring season. These surveys were conducted both upstream and downstream of the rock ramp and the Cass River dam from 2011 to 2016. Fish species abundance was measured in terms of catch per minute of electrofishing, and the data were compared between the upstream and downstream areas using a general linear model. As a reference for evaluating changes in adult fish distribution and abundance, the researchers used historical data from past summer and early autumn surveys. Before the installation of the rock ramp fishway in 2009, there were a total of 55 recorded species in the river, with 35 species present in both upstream and downstream regions, while 20 species had varying distributions. In their recent surveys, only seven of these 20 species with differing distributions were captured, all of which had historically been confined to the downstream region. During the electrofishing surveys conducted on the Shiawassee River, they captured 26 fish species, with 20 downstream and 23 upstream of the fishway. In the Cass River, they captured 40 species, with 38 downstream and 27 upstream of the dam. Regarding the distribution of fish eggs, 96% were collected downstream of the fishway in the Shiawassee River. In contrast, in the Cass River, the distribution of eggs was more evenly split, with 42% downstream and 58% upstream. Additionally, the researchers captured, marked, and released a total of 22,267 fish representing 13 species below the rock ramp. They observed more recaptures downstream than upstream, with only 14 upstream recaptures. These findings suggested the effectiveness of the fishway was limited, as catches were significantly higher below the fishway compared to above it. This indicated that the rock ramp fishway still posed some restrictions on upstream fish migration.

Nevertheless, overall connectivity improved compared to the completely dammed river, even though full connectivity was not achieved (Murry et al., 2020).

Richer et al. (2020) observed the performance of a rock ramp fishway set on a 5% slope within the Cache la Poudre River in Colorado, USA. They evaluated the effectiveness of the fishway for passing nine fish species with varying swimming abilities in two trials: a 46-hour enclosure study and a 3-month extended study. The target species for the fishway design were Brown Trout (*Salmo trutta*) which was the strongest swimmer, Longnose Dace (*Rhinichthys cataractae*), Longnose Sucker (*Catostomus catostomus*), and Brassy Minnow (*Hybognathus hankinsoni*) which was the weakest swimmer. The movement of these fish species was tracked using PIT tags. An overall passage success rate of 81% was documented during the enclosure study, with all the target fish species able to ascend it. However, the extended study yielded a diminished overall passage success rate of 19%, with only three of the four target species achieving successful passage. The decline in passage success was particularly pronounced among the fish species characterized by weaker swimming abilities. Specifically, during the enclosure study, Brown Trout exhibited a passage success rate of 96%, while Longnose Dace, Longnose Sucker, and Brassy Minnow displayed passage success rates of 51%, 98%, and 24%, respectively. In contrast, during the extended study, these passage success rates dropped to 51%, 5%, and 12%, respectively, with the Brassy Minnow not detected at the fishway during the extended study (Richer et al., 2020).

Passage studies on rock ramp fishways have provided valuable insights into the effectiveness of these structures in promoting fish passage and restoring ecological connectivity across diverse aquatic environments. While these investigations have highlighted the advantages

and limitations of rock ramp fishways, it is important to acknowledge that the full scope of their impact and potential is still a subject of ongoing research. The known benefits include improved fish passage, increased species richness, and the accommodation of fish of varying swimming abilities. However, the challenges in achieving complete connectivity for all targeted species indicate the need for continued research and refinement in rock ramp fishway design. Future studies should examine the effects of fish characteristics, such as size and swimming ability, fish condition, and environmental variables such as water temperature on passage performance. Additionally, continuous research and monitoring of these fishways are essential for assessing their long-term effects on fish communities and ecosystem connectivity. Evaluations like these are crucial in determining the overall influence of rock ramp fishways on the ecosystem. Moving forward, the combination of existing knowledge and ongoing research will contribute to further enhancing the effectiveness of rock ramp fishways, ultimately aiding in the conservation and restoration of fish populations and aquatic ecosystems.

Rock Ramp Fishway Hydraulics Studies

Some researchers have reported on the passage success of various fish species within rock ramp fishways. To comprehensively understand how these fish successfully navigate through the fishway, researchers have conducted an in-depth hydraulic analysis of the rock ramp fishway. These hydraulic studies focused on velocity, water depth, flow patterns, turbulence characteristics, and other flow hydraulics elements. They aim to understand how these hydraulic elements impact fish movements within rock ramp fishways. Additionally, these studies investigate the influence of boulders arrangement, concentration, and roughness on these

hydraulic dynamics. Hydraulic analyses have been achieved through physical model studies (using flumes or small channels to imitate large-scale water bodies) and/or CFD model studies.

Physical Model Studies

Pagliara & Chiavaccini (2006) investigated the flow resistance of rock chutes with protruding boulders. Their research assessed flow resistance in terms of both Manning's coefficient and Darcy-Weisbach's friction factor. These experiments were conducted in three flumes at the Hydraulic Laboratory of the University of Pisa in Pisa, Italy, each having varying dimensions and configurations. The researchers investigated the impact of different parameters, such as slope, relative submergence, and blocks configuration, on the hydraulic behavior of the structure. They arranged the protruding boulders in two distinct patterns: random and rows. The findings revealed that the presence of protruding boulders significantly increased the flow resistance, particularly when boulder concentrations were higher. Furthermore, the study highlighted that the boulder arrangement had a significant impact on the flow resistance, with the random arrangement inducing more resistance compared to the row arrangement. Additionally, the research indicated that the roughness of the boulders significantly contributed to flow resistance, with rougher boulders resulting in greater resistance. Following their experiments, the authors proposed new mathematical relationships to account for the impact of slope, boulder concentration, arrangement, and surface roughness on flow resistance in block ramps and constructed riprap channels on steep slopes. They also proposed new relationships to determine Darcy-Weisbach's friction factor and Manning's coefficient for standard base ramps (Pagliara & Chiavaccini, 2006).

Bretón et al. (2013) conducted experiments in a rock ramp fishway installed in a flume at the Hydraulics Laboratory of the University of Alberta in Canada. The flume had a smooth bed of 5% slope and a staggered arrangement of isolated emergent boulders at three different discharge rates. They studied turbulence and characterized the flow in the fishway using point and spatial analysis of time-series velocity data measured with an acoustic Doppler velocimeter (ADV). Point analysis included quadrant, autocorrelation, and spectral analysis of velocity time series, while spatial analysis included determining vorticity fields, Reynolds shear stresses, and higher-order velocity moments. The ADV was used to collect two types of data, a short time series of 2 minutes duration for the spatial analysis and a long time series of 30 minutes duration for the point analysis. The results from both analyses showed that velocity distribution was controlled by the geometry of the boulders' arrangement. Furthermore, there was high spatial variability presented by turbulence kinetic energy (TKE) and Reynolds shear stress distributions in the fishway. The researchers also found that velocity, vorticity, and kurtosis were low in the boulders' wake (downstream of boulders). This implied that the boulder wake could serve as a good resting zone for fish during passage through the fishway. Additionally, the spatial variability in velocity observed in the fishway suggests it can accommodate a diverse range of fish species by providing favorable paths for migration (Bretón et al., 2013).

Baki et al. (2014) conducted a study on the mean flow characteristics in a rock-ramp-type fishway, specifically focusing on a staggered arrangement of boulders. The objectives of the study included identifying the characteristic velocity regions in the fishway, developing general correlations for flow depth and velocity, and analyzing the flow resistance. The experimental setup consisted of a rock-ramp fishway installed in a rectangular smooth flume bed, with

boulders of approximately spherical shape. A total of 58 large cobbles, with diameters ranging from 12 to 16 cm, were glued to the bottom of the ramp. The experimental flume was adjusted to have different longitudinal slopes of 1.5%, 3%, and 5%. The researchers used a magnetic flow meter, ADV, and a yaw probe to measure water depth and velocity at various points. To assess the effect of the boulders on flow depth and velocity in the fishway, they compared the flow characteristics in the two channels. Baki et al. (2014) compared the flow characteristics in the fishway channel with that in a channel without boulders. The Manning equation, with a value of $n = 0.012$ for a smooth steel bottom, was used to estimate the flow depth and velocity in the channel without boulders. However, in the fishway channel, the flow depth was physically measured. The streamwise mean velocity was considered as the average velocity for this channel. The study found the presence of boulders in the fishway increased water depth by approximately three times compared to the channel without boulders. Additionally, the flow velocity in the fishway was reduced by about 64% compared to the channel without boulders. The study also identified three characteristic velocity regions in the fishway: downstream of boulders (wake region), upstream of boulders, and an intermediate region. Furthermore, the researchers developed correlations to predict the flow velocity in the rock ramp fishway based on normalized streamwise distance and discharge (Baki et al., 2014).

Cassan et al. (2014) conducted an experimental investigation to examine the hydraulic resistance associated with emergent macroroughness in fishways operating under high Froude numbers. They examined the influence of the boulder shapes, concentration, ramp slope, and bed roughness on the hydraulic resistance of fishways. The study took place at the Institute of Fluid Mechanics Toulouse (IMFT) in France and utilized two channels with varying dimensions and

slopes. The first channel, measuring 0.25 m in width and 10 m in length, featured a smooth polyvinyl chloride (PVC) bed to minimize roughness. Macroroughness was introduced in the form of wooden cylinders, 35 mm in diameter and 70 mm in height. The slope of the channel ranged from 1% to 8%, and data were collected under different flow conditions. In contrast, the second channel had a bed roughness consisting of pebbles ranging from 30 mm to 50 mm in diameter. Wooden cylindrical blocks, 115 mm in diameter and 150 mm high, were also used as macroroughness. Two different macroroughness concentrations, 13% and 16%, were evaluated, and the channel slope varied from 1% to 9%. Measurements were conducted across different flow rates and water levels. For both channels, the macroroughness was evenly distributed in staggered rows and protruded. Velocity measurements were taken at midwater depth, downstream of the boulder (or block) using an electromagnetic current meter and a miniature current flow meter. The Froude numbers under these tested conditions ranged from 0.14 to 1.80. Findings from the experimental observations indicated the flow pattern remained constant for a specific Froude number, although it exhibited some dependency on the water depth-to-block diameter ratio (h/D). Behind the blocks, a recirculation zone characterized by near-zero velocity was consistently observed. The width of this zone was approximately equivalent to the diameter of the block, while its length varied in relation to the Froude number. The results indicated that for low Froude numbers, the maximum water level was located upstream of the row of blocks, while for higher Froude numbers, it shifted downstream. Additionally, the study found the location of maximum velocity also moved downstream with increasing Froude numbers. Furthermore, the research proposed an analytical model for assessing hydraulic resistance in nature-like fishways, accounting for diverse geometric parameters such as block shape, ramp

slope, block density, and bed roughness. The experimental data were employed to validate and enhance this analytical model. The proposed analytical model was then utilized to refine the stage-discharge relationship for nature-like fishways. The study also emphasized the significance of considering the impact of the interaction between the wakes and the channel bed when analyzing fishway configurations (Cassan et al., 2014).

Baki et al. (2015) also investigated the turbulence characteristics generated in a rock ramp fishway model with a staggered arrangement of boulders. The researchers utilized the same experimental flume setup as described in Baki et al. (2014) for their study. The experiments were conducted at slopes of 1.5% and 3%, with different flow rates and submergence ratios. The research aimed to assess the impact of clusters of boulders and single boulders on turbulence magnitude and decay rate. Additionally, it sought to evaluate the suitability of rock-ramp fish passes for fish passage by examining various turbulence parameters. The turbulence parameters analyzed in this study included relative turbulence intensity, turbulent kinetic energy, Reynolds shear stress, mean turbulent statistics (skewness and kurtosis), energy dissipation rate, and dissipative eddy size. The researchers utilized statistical methods and power spectral analyses to analyze the turbulence characteristics. To measure three-dimensional (3-D) instantaneous velocity, they employed a Vectrino Plus ADV. The findings of the study revealed that the turbulence decay rate was slower in the wake-interference flow pattern generated by closely spaced boulders in the rock-ramp fishway compared to the isolated roughness flow pattern caused by single boulders. This was due to the neighboring boulders preventing the completion of vortex generation and dissipation before the next boulder. Consequently, the wake-interference flow pattern exhibited higher turbulence intensity and kinetic energy than the

isolated roughness flow. Additionally, they observed that the maximum values of turbulent kinetic energy and Reynolds shear stress in their study were higher than those reported in previous studies on flow around individual boulders and clusters of in-stream pebbles. However, the range between the highest and lowest values of turbulent kinetic energy and Reynolds shear stress was significantly lower. This was attributed to the flow hydraulics in the wake-interference flow pattern, which facilitated a higher dispersion of turbulence kinetic energy across the study area compared to an isolated single boulder. Based on their observations, the researchers concluded that the turbulence magnitude was highest when the boulders were closely spaced, indicating that the spacing between boulders influenced turbulence characteristics. They also established correlations for the streamwise turbulence intensity and turbulent kinetic energy as a function of normalized streamwise distance, offering a means to predict turbulence in a rock-ramp fish pass based on the spatial arrangement of boulders (Baki et al., 2015).

Meanwhile, Cassan & Laurens (2016) extended the research conducted by Cassan et al. (2014). The authors focused on two main objectives. The first objective was to simplify and modify the analytical model proposed by Cassan et al. (2014) for protruding macroroughness and extend its applicability to boulder arrangements with transverse and longitudinal spaces between blocks that are uneven. By comparing their experimental results with the proposed model by Cassan et al. (2014), they were able to propose a simpler version of the model that was able to accurately determine the geometry for irregular arrangements of blocks. The second objective was to develop an analytical model for submerged blocks. The researchers adapted one-dimensional (1-D) vertical models that were originally developed for vegetation to estimate the stage-discharge relationship and the velocities in different flow layers. They also proposed a

turbulence closure model to estimate the vertical velocity profiles and the turbulent viscosity for a wide range of block arrangements. The proposed model was compared to existing experimental stage-discharge correlations and was validated using data from the experiments. To achieve their results, the experiments were conducted in a down-scale physical model of a rectangular channel with varying slopes. The channel had a width of 0.4 m and a length of 4.0 m. Plastic cylinders with different heights were used as blocks in the channel. The blocks were arranged in various patterns with different densities. The flow rates and water depths were measured using cameras and electromagnetic flow meters (Cassan & Laurens, 2016).

Baki et al. (2017c) conducted a study on a submerged boulder in a boulder arrangement to investigate the mean and turbulent flow fields under a wake-interference flow condition. They utilized a similar experimental flume setup as described by Baki et al. (2014), but with a constant bed slope of 1.5%. The experiments were conducted under fully submerged conditions with different submergence ratios (H/D) ranging from 1.56 to 1.90. Flow conditions were modified by altering the discharge from 140 L/s to 198 L/s. To measure the three-dimensional instantaneous velocities, an ADV was used at a frequency of 100 Hz over a period of 3 minutes at each measurement point. The study observed that the streamwise velocity profile in the vertical direction displayed a similar trend around the boulder on all sides for all experiments. The maximum velocity was observed near the water surface, while the minimum velocity was found to be close to the bed. Similarly, the streamwise turbulence intensity profile showed a reasonable degree of similarity in each direction around the boulder. The maximum turbulence intensity magnitude was observed near the bed for the downstream side of the boulder, and near the water surface for the upstream and both sides of the boulder. These findings reveal the variations in

flow characteristics around the boulder in different areas. However, the profiles of the streamwise mean velocity, turbulence intensity, and the coefficient of correlation of velocity fluctuations had different shapes on each side of the boulder. The study proposed empirical relations for these profiles. The coefficients for these empirical relations were determined based on the experimental data obtained from the study (Baki et al., 2017c).

Cao et al. (2020) conducted a study to investigate how the interaction between boulders and bed permeability influences flow characteristics. Their research involved examining parameters such as the distribution of mean flow velocity, Reynolds stresses, and TKE. The experiments were conducted using a rectangular flume. The flume had dimensions of 0.5 m in width, 0.6 m in depth, and 16 m in length, with a channel bed slope of 0.1%. An inlet valve was used to control flow configurations, and a sharp-crested weir was used to measure the flow discharge. Three bed configurations were utilized for the study: smooth bed (SB), impermeable bed (IMPB), and permeable bed (PB). Glass beads with a diameter of 12 mm were used to create bed roughness, while 40 mm spherical plastic balls served as boulders. The IMPB referred to the bed with one layer of glass beads, while the PB had two layers. The boulders were arranged in a staggered pattern and buried in the glass-bead beds. A SonTek® 10 MHz ADV was used for the measurement of the 3-D instantaneous flow velocities. The findings from the study demonstrated that decreasing the height of the exposed boulders increased the bed permeability. This is because the height of exposed boulders determined the extent to which the flow could penetrate the bed and facilitate the exchanges of mass, momentum, and energy between the surface and subsurface regions of the bed. When boulders had a lower exposed height from the bed surface, it resulted in a reduction in the near-bed velocity gradient, indicating a decrease in the bed shear

stress. This reduction in the velocity gradient correlated with an increase in bed permeability as it allowed for greater flow exchange through the bed. However, the decrease in the exposed height of the boulders did not significantly impact the magnitude of the streamwise velocity. Furthermore, the study demonstrated bed permeability negatively affected the production, transport, and diffusion of the TKE. Specifically, they were smaller for the PB compared to the IMPB. While the study did not pinpoint the exact cause of this impact, it suggested that the increased bed permeability in the PB, relative to the IMPB, might have reduced turbulent activity in the vicinity of the boulders (Cao et al., 2020).

In the study conducted by Zheng et al. (2020), an investigation was carried out to assess how the permeability of partition walls within rock ramp fishways affects the hydraulic characteristics within these fishways. The partition wall refers to the inner wall structure that divides the fishway, that is, the rows of obstacles dividing the fishway. To conduct their analysis, the researchers utilized a trapezoidal flume with a bed slope of 1% and a side slope of 1:2.5. They examined flow velocity and flow patterns in three different types of permeable partition walls: impermeable partition wall (IPW), semi-permeable partition wall (SPPW), and fully permeable partition wall (FPPW). Cobbles with diameters ranging from 10 cm to 15 cm were used to simulate the permeable walls, while a brick wall represented the impermeable walls. The SPPW consisted of a bottom impermeable layer and a top permeable layer. The roughness of the fishways was also defined using Manning's roughness coefficient (n). The researchers established a relationship between flow velocity, discharge, and channel roughness. Their findings indicated that as discharge increased, velocity also increased while roughness decreased. The experimental data revealed that fishways with IPW exhibited the highest roughness,

followed by SPPW, and FPPW demonstrated the lowest roughness. According to the relationship they established, this suggested that the flow velocity and discharge in the channel with IPW were the lowest. Considering that the discharge in fishways with SPPW fell in between, it implied that SPPW fishways allowed for a moderate level of water flow, which is crucial for operational efficiency. The authors observed IPW led to flow characteristics similar to those found in engineered technical fishways. Consequently, they recommended the construction of rock ramp fishways with SPPW due to the tendency of IPW to create recirculation flow zones that impede fish migration (Zheng et al., 2020).

Mao et al. (2021) investigated the flow characteristics and energy dissipation rates within nature-like fishways. Physical models were employed to analyze and compare the velocity distributions for two fishway types, denoted as Type I and Type II. Both fishways utilized impermeable partition walls. In the Type I fishway, these partition walls were alternated, with one row featuring the partition wall near the left bank and the subsequent row having the partition wall near the right bank. This configuration created a single primary flow path for each row of obstacles. In contrast, the Type II fishway featured partition walls positioned side by side, constricting the flow within one row, while the next row had a single partition wall in the center. This arrangement in the Type II fishway resulted in two primary flow paths, one near the left bank and the other near the right bank. The study primarily focused on the migratory fish species, *Schizothorax oconnoris* and *Schizothorax macropogons*. Their optimal swimming speeds were determined. Adjustments to the water depth in the fishways were made in accordance with the ecological habits of these target fish species. Additionally, the slope of the fishways was maintained within 2%. Velocities were measured using a micro propeller flow

meter, with the vertical average velocity of a measuring point calculated using the three-point method. This method involves calculating the mean velocity by averaging the velocity obtained at 0.2 and 0.8 of the total water depth from the surface, and then averaging that result with the velocity recorded at 0.6 of the water depth (U.S. Geological Survey, 2019). The study's findings revealed that the maximum flow velocity in the Type II fishway was approximately 5.64% higher than that observed in Type I. The researchers attributed this to the narrowing of the flow path by the obstacles in Type II, leading to an increase in velocity in the constriction. However, the average flow velocity in the Type I fishway exceeded that of Type II by 21.1%. Furthermore, the volumetric energy dissipation rate was quantified at 26.8 W/m^3 for the Type I fishway and 25.1 W/m^3 for the Type II fishway (Mao et al., 2021).

In a study conducted by Swarr et al. (2023) at the Colorado State University Foothills Fisheries Laboratory, an investigation was carried out on the hydraulic characteristics of a newly designed and constructed model rock ramp fishway. The study utilized a specially constructed flume with an adjustable slope, designed to accommodate a full-scale fish passage structure. The flume comprised two segments, each measuring 4.55 m in length, which could be bolted together to create a 9.1 m long experimental channel. The primary objective of this flume setup was to facilitate controlled laboratory experiments on fishway design and functionality prior to their real-world implementation, thereby saving time and money. Within this flume, a prototype fishway was developed to cater to small-bodied fish species of conservation concern. The fishway featured a trapezoidal cross-section with side slopes inclined at 30° and a central channel width of 0.61 m. The macroroughness elements for the fishway were created using roughly hemispherical polyethylene rocks, each measuring approximately 95 mm in diameter and 55 mm

in height. These rocks were arranged in a chevron pattern with a spacing equivalent to one diameter. To assess the hydraulics of the fishway, the researchers measured the mean water velocity and water surface elevations (WSEs) at different points within the fishway at various slopes and flow rates. The mean water column velocity was quantified using a Marsh McBirney flowmeter, while WSEs were measured at approximately 60% of the water depth using a point gauge. These measurements were taken upstream, downstream, and between roughness elements. The findings of the study revealed significant variations in mean water velocities across different slope treatments, with higher velocities observed at steeper slopes. However, there was no significant difference in mean water velocity between slopes of 2% and 4%. Additionally, the study noted relatively consistent WSEs within the fishway for each slope treatment, with slightly higher elevations observed in fishways with steeper slopes. This variation in elevation was attributed to turbulence generated among the roughness elements. Overall, the results of the study indicated the model rock ramp fishway successfully created satisfactory hydraulic conditions conducive for fish passage (Swarr et al., 2023).

These numerous studies have provided valuable insights into the complex interactions between flow characteristics and structural elements within fishways. Researchers have examined various factors, including the arrangement and shape of boulders, bed roughness, permeability of partition walls, and slope. These studies have shed light on the impact of boulder elements configuration on flow resistance, turbulence, and energy dissipation within rock ramp fishways. However, several aspects of rock ramp hydraulics remain unclear and require further exploration. One such area of interest is the influence of bed permeability on flows deflected by boulders. Bed permeability refers to the ability of the channel bed, typically composed of

sediment or pebbles, to allow water to flow through it. Water seeping through the bed due to high permeability might affect the flow deflection patterns around the boulder structures. This can subsequently influence turbulence and energy dissipation, overall modifying the hydrodynamic conditions around the boulders. More permeable beds can potentially slow down the water velocities around the boulders, enabling the fish to swim around these obstructions more easily. Moreover, there is a need for additional research focused on flow characteristics in the vicinity of submerged boulders. This research should encompass different boulder densities to replicate the wake-interference flow regime and diverse bed configurations. Furthermore, it is imperative to conduct field studies to validate the laboratory findings and to assess the long-term performance of these nature-like fishways in real-world conditions. Additionally, a more holistic perspective is required to comprehend the overall ecosystem function of these fishways. This entails incorporating ecological factors such as habitat suitability, sediment and debris transport, and water quality into the analysis of flow characteristics. The results from these experiments will be useful to fish passage engineers and biologists to understand the effects of hydraulic and turbulence characteristics in relation to fish passage.

CFD Model Studies

Baki et al. (2016) employed the commercial software, ANSYS-CFX, in their research to explore the impacts of boulder size, pattern, and channel slope on the hydraulic characteristics of a rock ramp fishway. They built upon the results from the physical modeling done by Baki et al. (2014). This software, utilizing a finite volume method, solves 3-D Reynolds-averaged Navier-Stokes (RANS) equations. The ANSYS-CFX software is multiphasic, enabling the modeling of the free surface between air and water using the volume of fluid (VOF) technique. The authors

used the standard k-ε turbulence model to predict the turbulent viscosity in their numerical simulations. A sensitivity analysis of the initial water level was conducted and found to have negligible effects on the simulated water levels. Additionally, a mesh independence study was conducted for one of the simulations to evaluate the influence of different mesh sizes on simulation accuracy. By comparing the results obtained from the physical model with those from the numerical model, the researchers observed a close match in simulated water levels and flow velocity profiles. However, disparities between observed and simulated flow velocities were identified in the wake region. They attributed this discrepancy to turbulence-induced adverse pressure gradients and recirculation within the wake zone. Furthermore, there was poor agreement between observed and simulated TKE values in the wake region. The study suggested that this lack of agreement could be potentially influenced by factors such as natural boulder size and shape variations, measurement uncertainties, and the choice of turbulence model in the numerical simulations. This study also developed a general correlation to estimate average water depth in rock ramp fishways as a function of normalized discharge (Baki et al., 2016).

Baki et al. (2017a) aimed to examine the impact of variations in structure geometry and channel properties on the hydraulic behavior of rock-weir fishways. Additionally, they sought to develop general relationships for predicting depth-discharge and maximum velocity based on structure geometry. Their numerical model was designed to replicate the experimental work conducted by Kupferschmidt & Zhu (2017) for a rock-weir fishway. The computational domain included a rock-weir fishway measuring 0.92 m in width, 0.61 m in height, and 9 m in length, consisting of five pools formed by six rock-weirs. These weirs were arranged in three different configurations: layout (I) with the V-weir facing upstream, layout (II) with the V-weir facing

downstream, and layout (III) with horizontal weir perpendicular to the flume walls. The simulations were conducted using ANSYS-CFX and implemented the Volume of Fluid (VOF) method to model the free surface between air and water. To assess the numerical model's performance, the researchers compared their results with the experimental data on water depth and velocity obtained from the study conducted by Kupferschmidt & Zhu (2017). The findings demonstrated that the simulations effectively reproduced the water surface profiles and flow patterns for the various weir configurations and flow conditions. The results revealed that layout (I) directed flow recirculation toward the banks of the channel rather than the center of the pool. Conversely, layout (II) directed flow toward the channel sides, causing recirculation in the center of the pool as opposed to along the channel banks. Layout (III) exhibited flow directions perpendicular to the channel cross sections, with minor convergences and divergences occurring upstream and downstream of the weir, respectively. Consequently, fewer flow recirculation zones were observed along the channel banks in layout (III) compared to layout (I). As a result, layout (I) was deemed suitable for fish swimming along the channel center, while layouts (II) and (III) were recommended for locations where fish preferred to swim along the channel banks. Through their analysis of flow patterns, the researchers identified three distinct flow regimes: weir flow, transitional flow, and streaming flow, all of which were influenced by channel characteristics and structural geometry. Additionally, the study introduced a new depth-discharge relationship expressed in terms of upstream head. Furthermore, the researchers proposed a modified equation for predicting maximum velocity in nature-like rock-weir fishways, building upon an existing maximum velocity equation (Baki et al., 2017a).

To provide a design evaluation and considerations for rock-weir fishways, Baki et al. (2017b) conducted research based on the findings and simulations from another study by Baki et al. (2017a). Their primary focus was to investigate how various channel characteristics and structure geometries affect water depth, flow velocity, and the location of slow velocity zones crucial for fish resting. The numerical simulations were conducted using ANSYS-CFX, employing the same numerical setup, rock-weir layouts, and experimental validation data used in Baki et al. (2017a). The study quantified the influence of channel characteristics and geometry on flow depth by calculating the ratio of water depths with and without rock-weir (H/H_0) within the fishway. It was observed that the presence of weir structures led to pool depths that were 3.0-5.6 times greater than the normal depth (H_0). As the flow rates increased, the study noted that the pool depth ratios decreased, indicating a change in the flow regime. Additionally, an increase in the bed slope resulted in a corresponding increase in the pool depth ratios, while raising the weir height substantially increased the pool water depths. In evaluating the impact on flow velocity, the researchers introduced the concept of the maximum velocity reduction factor (η), expressed as $\eta = 100 \times (V_0 - U_{max})/V_0$. V_0 represents the velocity without rock-weirs and U_{max} denotes the maximum velocity in the rock-weir fishway. They observed that increasing flow rates correlated with a decrease in the maximum velocity reduction factor, while an increase in bed slope led to an increase in this reduction factor. Pool spacing also played a role, with shorter distances between pools resulting in a more significant reduction factor. However, increasing the weir height had minimal influence on the velocity reduction factor. Furthermore, the study examined the zones of slow velocity within the fishway, which are important for fish resting. The findings indicated that the orientation of the weir structures had a negligible effect on the availability of

these slow velocity zones. Based on their findings, the authors provided recommendations for design procedures for effective rock-weir fishways (Baki et al., 2017b).

Chorda et al. (2019) conducted a study that employed numerical modeling to investigate the flow characteristics within a fishway. The primary objective of the research was to utilize CFD models to predict complex flow behaviors in a fishway, specifically focusing on the design of efficient rock ramp fishways for small fishes. The authors utilized the open-source code OpenFOAM to simulate free surface flow across a steep-sloped ramp covered with staggered surface emergent cylinders. Two turbulence models, shear stress transport (SST) k-ω and Smagorinsky large-eddy simulation (LES), were applied in their numerical modeling. The study used two computational meshes, coarse (Mesh1) and fine (Mesh2), to examine the flow patterns around the obstacles and the wake interactions between rows. Mesh1 represented a configuration with eight rows of obstacles, while Mesh2 was a configuration with four rows of obstacles. These computational meshes were generated using the open-source SALOME software platform. For the numerical model setup, the experimental setup previously described by Tran et al. (2016) was replicated. This setup entailed a flume with a width of 1.0 m, a streamwise slope of 5%, a spatial arrangement of cylinders at a concentration of 16%, and a discharge rate of 0.05 m^3/s. The researchers compared and validated their numerical models using experimental data from Tran et al. (2016). The study outcomes indicated that coarse Mesh1 model coupled with SST k-ω turbulence model provided accurate time-averaged values for various flow parameters and fluctuations. This made it a suitable choice for designing rock ramp fishways. However, it was observed that this model combination tended to overestimate the horizontal velocity (U values) in the wake zones. The fine Mesh2 model using the SST k-ω model improved the precision in

these zones. On the other hand, the fine Mesh2 model employing the LES turbulence closure yielded more intricate flow information, especially within the wakes. This level of detail was particularly valuable when considering potential fish resting zones for smaller fish. In summary, the study utilized the SST k-ω turbulence model with coarse Mesh1 for the overall analysis of flow behavior and the LES turbulence model with the fine Mesh2 to capture detailed flow features. In essence, the research effectively showcased the capability of CFD in predicting complex flow characteristics within fishways (Chorda et al., 2019).

Baki et al. (2020) carried out a numerical investigation into the impact of various notch sizes and configurations on flow patterns and hydraulic characteristics in rock-weir fishways. Their research methodology was based on the earlier work of Kupferschmidt & Zhu (2017), Baki et al. (2017a), and Baki et al. (2017b), which focused on flow characteristics in rock-weir fishways but did not consider passage notches. For their numerical simulations, Baki et al. (2020) employed the ANSYS-CFX software and utilized the VOF technique in combination with the k-ε turbulence model. The researchers applied a validated numerical model from their previous work, Baki et al. (2017a). For their study, they utilized a rock-weir configuration featuring a V-weir facing upstream, composed of large cobbles measuring 0.14 m in diameter. Smaller cobbles with a 0.07 m diameter were used to create the notches. They explored three different notch configurations: setup (I) with notches alternating on both sides of the "V"s, setup (II) with notches on the same side of the "V"s, and setup (III) with notches on both sides of the "V"s. The width of the notches ranged from 0.08 to 0.38 times the width of the channel. Comparing the longitudinal water surface profiles along the centerline of the channel in their study with those presented in Baki et al. (2017a) for a V-weir facing upstream without notches, it

was observed that the presence of notches in the rock weirs resulted in a reduction in water depth and an increase in maximum weir velocity compared to structures without notches. Additionally, they observed that in setup (I), with notches near the center channel, the flow recirculation zone was slightly larger compared to setup (I) with notches near the side channel, resulting in reduced slow velocity zones near the center channel. In setup (II), the maximum velocity increased by approximately 9% due to reduced backwater effects, and the area of slow velocity expanded as flow was concentrated on one side of the pool. In contrast, in setup (III), the flow recirculation zones elongated along both banks, leading to larger slow velocity areas. Furthermore, the size of the notches also influenced the flow patterns and slow velocity zones. Increasing the size of the notches led to a reduction in the average percentage of slow velocity zones. Increasing notch sizes were associated with greater maximum velocity magnitudes and larger flow recirculation zones within the pools. However, the researchers noted that compared to notch configuration, the influence of notch sizes was relatively minor. In summary, the study highlighted that the configuration of notches, specifically their alignment and orientation, had a significant impact on the distribution of slow velocity zones within rock-weir fishways (Baki et al., 2020).

Miranda et al. (2021) conducted a study to explore the significance of boulder shape in a rock ramp fishway and sought to demonstrate the capability of CFD in predicting flow behaviors within fishways. The researchers conducted both physical experiments and numerical simulations for a rock ramp fishway with staggered emergent square obstacles. They validated their CFD model by replicating an experimental setup described by Cassan et al. (2014) but using square-shaped obstacles. Then, the numerical results of the velocity field and TKE were compared with their experimental measurements. To investigate the effect of boulder shape,

Miranda et al. (2021) specifically replicated a scenario with circular (cylindrical) obstacles, as previously analyzed by Chorda et al. (2019), but with square obstacles. The results from both their square obstacle simulation and the circular obstacle simulation performed by Chorda et al. (2019) were compared and analyzed. In their numerical simulations, the authors utilized the open-source code OpenFOAM, applying the Smagorinsky-based LES turbulence model. Additionally, they employed the VOF method to model the free surface, and mesh generation was accomplished using the open-source software SALOME. The findings revealed a minor discrepancy in the wake region of the velocity profile, where the numerical simulation exhibited a shorter wake zone compared to the experimental observations. However, the discrepancies in TKE between the numerical results and experimental measurements were minimal. Both the numerical and experimental results for velocity profiles and TKE exhibited similar values and behavior, indicating a good agreement. Regarding the impact of boulder shapes, the study outcomes revealed that square-shaped obstacles resulted in a lower velocity field, reduced TKE, and fewer lateral fluctuations, indicating better passability for fish compared to circular obstacles. However, square-shaped obstacles which led to increased water depth resulted in a smaller discharge. This configuration could potentially make discharge less appealing for fish. Overall, these findings highlighted the importance of considering obstacle shapes in the design of fish passages (Miranda et al., 2021).

Great Plains Fish Species of Interest

In the streams of the Great Plains of North America, there exists a diverse range of fish species, varying in both size and swimming abilities. The current study focuses on the same fish species that were examined in the physical experimental research performed by Swarr (2018).

The selection of these species was based on their availability and accessibility of prior swimming performance data. These fish species include Flathead Chub (*Platygobio gracilis*), Arkansas Darter (*Etheostoma cragini*), and Stonecat (*Noturus flavus*). These species are characterized by their small size, with a total length (TL) spanning from 47 mm to 213 mm and mass ranging from 0.94 g to 121.22 g. They are indigenous to the Great Plains region (Swarr, 2018). In the laboratory experiment conducted by Ficke et al. (2011), Arkansas Darters were placed in a swim tunnel and subjected to various test velocities. The aim was to assess their swimming performance using an endurance test protocol. The findings revealed that Arkansas Darters were poor swimmers, poor jumpers, and bottom oriented. They were easily displaced when exposed to high water velocities. Based on the study findings, the researchers recommended that velocity in fishways should not exceed 32 cm/s (0.32 m/s) for Arkansas Darters (Ficke et al., 2011). In a separate investigation conducted by Ficke (2015), Flathead Chubs and Stonecats were introduced into a swim tunnel. These fish were subjected to both constant acceleration tests and fixed velocity tests to ascertain their swimming speeds. The constant acceleration tests involved steadily increasing the water velocity within the swim tunnel at a constant rate until the fish in it became exhausted. Whereas in the fixed velocity tests, the current velocity in the swim tunnel was set to a constant value, and the fish swam at this velocity until exhaustion. From the outcome of the study, Flathead Chubs were classified as excellent swimmers, with a sprint swimming speed of 114 cm/s (1.14 m/s). On the other hand, Stonecats were categorized as moderate swimmers, with a sprint speed of 62 cm/s (0.62 m/s) (Ficke, 2015).

Discussion

Dam construction on stream and river systems has negative impacts on the aquatic ecosystem, including stream fragmentation. This fragmentation has been particularly evident in the Great Plains of North America, leading to declines in the population of small-bodied fish species endemic to the region. In addition, dams create favorable conditions for the invasion of non-native species, further disrupting native fish communities. Rock ramp fishways have been evaluated for their effectiveness in promoting fish passage and restoring river connectivity.

Studies on rock ramp fishways, both in physical models and CFD models, have provided a good understanding of the hydraulic characteristics and flow patterns within these fish passage structures. The studies analyzed factors such as boulder size, pattern, channel slope, and geometry of the fishway, and their impact on flow depth, velocity, and turbulence characteristics within the fishway. The findings indicated the design of fish passages significantly influences the flow patterns and hydraulic behavior within the fishway. These studies have also identified favorable fish resting zones within the fishway, such as the boulder wake, which can enhance the passage success for fish. While these studies provided important insights into fish passage, they predominantly focused on larger fish species known for their strong swimming abilities, jumping skills, and commercial values.

Building upon the experimental study conducted by Swarr (2018), the current study will utilize CFD model to explore the impact of varying the bed slope and flow rate in a rock ramp fishway on the passage of three species of small-bodied fish found in the Great Plains. Each of these fish species exhibits different swimming performances. The physical experiments were conducted using a 6.1 m long rock ramp fishway installed in a 9.1 m long flume. The flow depth

and velocity data from the physical observations will be used to validate the capability of the CFD model to replicate real world conditions. By evaluating the flow depths, velocities, and TKEs, this study aimed to better understand the hydrodynamics in rock ramp fishways that will benefit juvenile fishes, small-bodied fishes, and fishes with weak swimming speed. Additionally, the study will illustrate the benefits of integrating findings from physical models and CFD models to gain a more comprehensive understanding of fish passage hydraulics, especially for small fishes. This study is intended to contribute to existing knowledge that will help engineers build more effective rock ramp fishways to restore and improve stream connectivity for all aquatic creatures, irrespective of size and swimming ability.

CHAPTER TWO: ROCK RAMP MODELING

Introduction

With the increasing need for water control and management, hydraulic structures such as dams, culverts, and instream modifications have become an integral part of river systems worldwide. While these structures provide benefits for human activities such as water storage, flood control, irrigation, and power generation, they also negatively impact aquatic ecosystems (Özkaya, 2014; Quaresma & Pinheiro, 2014; Koçal, 2019). Stream fragmentation caused by instream structures disrupts the natural connectivity of streams and rivers, leading to habitat destruction, ecological hazards, and displacement of fish populations. Many water bodies in the Great Plains of North America are impacted by stream fragmentation. With over 19,000 instream structures, not including culverts, constructed on streams in this region, the fragmentation has initiated a concerning shift toward increasingly homogenized fish communities and highly regulated streams (Perkin et al., 2015). The primary concern related to fragmentation is the hindrance caused by the anthropogenic barriers to the upstream movement of migratory Great Plains fish species. To mitigate the upstream movement impediment and restore longitudinal stream connectivity, fish passage structures (also known as fishways) are installed at barriers (Romão et al., 2017; Baharvand & Laskar-Ara, 2021).

Fishways are specialized hydraulic structures designed to assist migratory fish in bypassing or overcoming obstacles such as dams, culverts, or other barriers within regulated waterways (An et al., 2016). These fishways can be either technical or nature-like fishways. Technical fishways are constructed using engineered materials and feature stepped channels with flat surfaces (Katopodis et al., 2001; Stoller et al., 2016). In contrast, NLFs are built with natural

materials like rocks, gravel, boulders, riparian vegetation, and wood to mimic the geomorphological characteristics of natural stream channels (Zheng et al., 2020).

Fish passage studies have focused primarily on large diadromous fishes, particularly economically important fish species such as salmonids. However, to ensure the success of fishways in facilitating upstream movement for all fish species, regardless of their size, there is now growing emphasis on modifying fishway designs to accommodate small-bodied fish (Mallen-Cooper & Stuart, 2007; Silva et al., 2018). Among the several types of fishways, rock ramp fishways have gained recognition as the preferred option to enhance the upstream passage efficiency of small-bodied fish (Swarr, 2018; Stuart & Marsden, 2021). The performance and effectiveness of these structures are highly dependent on the hydrodynamics within them.

While there have been numerous studies of the performance of rock ramp fishways and their effectiveness in restoring longitudinal connectivity, there is still a need to enhance the understanding of the hydraulic conditions within this fishway. Physical modeling has been the main approach to studying hydrodynamics in rock ramp fishways. Bretón et al. (2013), Baki et al. (2014), Baki et al. (2015), Zheng et al. (2020), Mao et al. (2021), and others have studied the flow and turbulence characteristics in physical rock ramp fishways. However, physical experiments can be time-consuming and expensive to construct. Therefore, with the advancement in computer technology, the use of three-dimensional (3D) Computational Fluid Dynamics (CFD) models has become more prevalent for studying flow patterns within fish passage structures.

Computational fluid dynamics is a subfield of fluid mechanics that involves analyzing the dynamics of fluid flows using numerical methods. The Navier-Stokes equations are non-linear

partial differential equations that govern the motion of fluids. Due to their complexity, these equations cannot be solved analytically for most real-world problems. By implementing a CFD model, researchers and fishway designers can predict crucial parameters like water velocity, turbulence, and pressure distribution within the fishway. This data is vital to understanding the energy expenditure required by the fish, the potential stresses they could face, and, overall, the survivability of the species using the passage (Carrero-Díez et al., 2022). The interplay of these parameters, coupled with species-specific characteristics, makes CFD an indispensable tool in optimizing the design and operation of these fishways, thus contributing significantly to conservation efforts. Baki et al. (2016) used the CFD software, ANSYS-CFX, to investigate the effects of bed slopes, boulder size, and arrangement on the hydraulic parameters of a rock ramp fishway. Duguay et al. (2017) and Fuentes-Pérez et al. (2022) compared the capabilities of two CFD software packages, OpenFOAM and Flow-3D, in modeling flow in a pool and weir and vertical slot fishways, respectively. Quaresma et al. (2018) and Tan et al. (2021) utilized Flow-3D in their respective fishways studies, while Kalathil & Chandra (2023) employed Flow-3D Hydro software in their step-pool NLF study.

This study aims to contribute to the existing body of knowledge by utilizing CFD modeling to comprehensively assess the hydraulic conditions within a rock ramp fishway. By simulating and analyzing the complex flow patterns and parameters, valuable insights into the performance and effectiveness of rock ramp fishways will be gained. Furthermore, this research builds upon the study conducted by Swarr (2018), which utilized a rock ramp fishway installed in a custom-made adjustable full-scale flume at the Colorado State University Foothills Fisheries Laboratory (CSU FFL) to assess fish passage efficiency at different slopes and flow rates. By

employing a CFD approach, this study aims to simulate and further investigate the hydrodynamic conditions within the fishway. By analyzing flow patterns, water velocities, and their impact on successful fish passage, a comprehensive understanding of the effectiveness of rock ramp fishways for small-bodied fishes in the Great Plains regions of North America can be gained. Also, this research will showcase the capabilities of CFD in accurately predicting complex flow features.

CFD Theory

The CFD modeling for this study was conducted using Flow-3D Hydro (version 2023R1), a commercial software developed by Flow Science (2023). Flow-3D Hydro is a specialized version of FLOW-3D specifically designed to simulate water flow and related phenomena. It utilizes the Finite Difference Method (FDM) or the Finite Volume Method (FVM) to solve the Navier-Stokes equations. The flow region is discretized into a mesh of fixed rectangular cells, and control volumes are used to compute surface fluxes and forces for numerical approximations. The Navier-Stokes equations consist of two primary equations: the conservation of mass and the conservation of momentum equations. The governing equations used by Flow3D Hydro are in the form shown below:

Conservation of Mass Equation (General form):

$$V_F \frac{\partial \rho}{\partial t} + \frac{\partial}{\partial x}(\rho u A_x) + \frac{\partial}{\partial y}(\rho v A_y) + \frac{\partial}{\partial z}(\rho w A_z) = R_{DIF} + R_{SOR} \quad (2.1)$$

Momentum Equations:

$$\frac{\partial u}{\partial t}+\frac{1}{V_F}\left\{uA_x\frac{\partial u}{\partial x}+vA_y\frac{\partial u}{\partial y}+wA_z\frac{\partial u}{\partial z}\right\}$$

$$=-\frac{1}{\rho}\frac{\partial p}{\partial x}+G_x+f_x-b_x-\frac{R_{SOR}}{\rho V_F}(u-u_w-\delta u_s) \tag{2.2}$$

$$\frac{\partial v}{\partial t}+\frac{1}{V_F}\left\{uA_x\frac{\partial v}{\partial x}+vA_y\frac{\partial v}{\partial y}+wA_z\frac{\partial v}{\partial z}\right\}$$

$$=-\frac{1}{\rho}\frac{\partial p}{\partial y}+G_y+f_y-b_y-\frac{R_{SOR}}{\rho V_F}(v-v_w-\delta v_s) \tag{2.3}$$

$$\frac{\partial w}{\partial t}+\frac{1}{V_F}\left\{uA_x\frac{\partial w}{\partial x}+vA_y\frac{\partial w}{\partial y}+wA_z\frac{\partial w}{\partial z}\right\}$$

$$=-\frac{1}{\rho}\frac{\partial p}{\partial z}+G_z+f_z-b_z-\frac{R_{SOR}}{\rho V_F}(w-w_w-\delta w_s) \tag{2.4}$$

Where V_F is the cell fractional volume, ρ is the fluid density, u, v, and w are the fluid velocity components in the x, y, z directions, A_x, A_y, and A_z are the fluid fractional areas in the corresponding directions, p represents the pressure, and R_{DIF} and R_{SOR} are the turbulent diffusion and the mass source terms respectively. Additionally, G_x, G_y, and G_z are the gravitational body forces, f_x, f_y, and f_z are the viscous accelerations, b_x, b_y, and b_z signify the flow losses in a porous media, u_w, v_w, and w_w are the source component velocities, and u_s, v_s, and w_s are the fluid velocities at the source surface relative to the source itself, all in the x, y, and z directions. Finally, δ is a coefficient that characterizes the pressure type of the source, with $\delta = 0$ and $\delta = 1$ signifying stagnation pressure type and static pressure type, respectively.

This study assumed an incompressible fluid where the density is constant. Hence, Equation (2.1) is reduced to the form:

Conservation of Mass Equation (Incompressible Fluid):

$$\frac{\partial}{\partial x}(uA_x) + \frac{\partial}{\partial y}(vA_y) + \frac{\partial}{\partial z}(wA_z) = \frac{R_{SOR}}{\rho} \tag{2.5}$$

To simulate flow through and around complex geometry without resorting to unstructured body-fitted meshes, Flow-3D Hydro employs the FAVOR method. FAVOR, standing for Fractional Area/Volume Obstacle Representation, is a method for representing solid geometry on a regular Cartesian grid. It assigns fractional area and volume values to each cell in the grid to represent the fraction of the cell occupied by the solid geometry. This method is well-suited for simulating complex geometries with sharp corners and narrow passages. The FAVOR™ method uses the V_F, A_x, A_y, and A_z terms.

Furthermore, the Volume of Fluid (VOF) method, initially described by Hirt & Nichols (1981), was employed to model the free surface. It is a numerical technique that simulates two or more immiscible fluids by tracking the distribution and movement of the fluid in each cell throughout the computational domain. The VOF function is represented by the symbol F (x, y, z, t) and satisfies the equation below:

Volume of Fluid Equation:

$$\frac{\partial F}{\partial t} + \frac{1}{V_F}\left[\frac{\partial}{\partial x}(FA_x u) + \frac{\partial}{\partial y}(FA_y v) + \frac{\partial}{\partial z}(FA_z w)\right] = F_{DIF} + F_{SOR} \tag{2.6}$$

Where F_{DIF} is the turbulent diffusion term and F_{SOR} is the volumetric source term for the fluid being simulated in a multiphase flow system. The rock ramp fishway was a free surface condition and was solved as one fluid, which was water. The VOF technique allows for the modeling of free surfaces by representing the volume fraction occupied by the fluid in each cell, with $F = 0$ representing a cell that is completely filled with air (voids) and $F = 1$ representing a cell that is completely filled with water. Applying the One Fluid VOF approach to the numerical modeling of the rock ramp fishway solves the continuity and momentum equations only for cells with water. This approach assumes that the gas phase (air), which is assigned a constant uniform pressure, has no influence on the liquid phase other than applying pressure on the free surface. Utilizing this approach offers several advantages. It enables a reduction in the size of the computational domain, leading to decreased run times, and simplifies the definition of mesh boundary conditions.

Flows in rock ramp fishways exhibit high turbulence and to accurately model their behavior, a two-equation turbulence model was employed. The selected model is based on Renormalization-Group (RNG) methods. The RNG model consists of two transport equations, turbulent kinetic energy (k) and its dissipation rate (ε), and it applies statistical methods to derive the averaged equations for turbulence quantities. The model offers broader applicability compared to the standard k-ε model. This is primarily because the constants used in the equations of the k-ε model, which are typically determined through empirical means, are explicitly calculated in the RNG model. The advantage of utilizing a two-equation turbulence model is that each equation will describe the two essential variables that characterize turbulence: length and time scales. The turbulence equations are shown below:

Turbulence Transport Equations:

$$\frac{\partial k}{\partial t} + \frac{1}{V_F}\left\{uA_x\frac{\partial k}{\partial x} + vA_y\frac{\partial k}{\partial y} + wA_z\frac{\partial k}{\partial z}\right\} = P_T + Diff_k - \varepsilon \tag{2.7}$$

$$\frac{\partial \varepsilon}{\partial t} + \frac{1}{V_F}\left\{uA_x\frac{\partial \varepsilon}{\partial x} + vA_y\frac{\partial \varepsilon}{\partial y} + wA_z\frac{\partial \varepsilon}{\partial z}\right\} = \frac{C_{DIS1}\cdot\varepsilon}{k}P_T + Diff_\varepsilon - C_{DIS2}\frac{\varepsilon^2}{k} \tag{2.8}$$

$$P_T = \left(\frac{\mu}{\rho V_F}\right)\left\{\begin{array}{c} 2A_x\left(\frac{\partial u}{\partial x}\right)^2 + 2A_y\left(\frac{\partial v}{\partial y}\right)^2 + 2A_z\left(\frac{\partial w}{\partial z}\right)^2 \\ +\left(\frac{\partial v}{\partial x}+\frac{\partial u}{\partial y}\right)\left[A_x\frac{\partial v}{\partial x} + A_y\frac{\partial u}{\partial y}\right] \\ +\left(\frac{\partial u}{\partial z}+\frac{\partial w}{\partial x}\right)\left[A_z\frac{\partial u}{\partial z} + A_x\frac{\partial w}{\partial x}\right] \\ +\left(\frac{\partial v}{\partial z}+\frac{\partial w}{\partial y}\right)\left[A_z\frac{\partial v}{\partial z} + A_y\frac{\partial w}{\partial y}\right] \end{array}\right\} \tag{2.9}$$

$$Diff_k = \frac{1}{V_F}\left\{\frac{\partial}{\partial x}\left(v_k A_x\frac{\partial k}{\partial x}\right) + \frac{\partial}{\partial y}\left(v_k A_y\frac{\partial k}{\partial y}\right) + \frac{\partial}{\partial z}\left(v_k A_z\frac{\partial k}{\partial z}\right)\right\} \tag{2.10}$$

$$Diff_\varepsilon = \frac{1}{V_F}\left\{\frac{\partial}{\partial x}\left(v_\varepsilon A_x\frac{\partial \varepsilon}{\partial x}\right) + \frac{\partial}{\partial y}\left(v_\varepsilon A_y\frac{\partial \varepsilon}{\partial y}\right) + \frac{\partial}{\partial z}\left(v_\varepsilon A_z\frac{\partial \varepsilon}{\partial z}\right)\right\} \tag{2.11}$$

$$\mu = \rho(\nu + \nu_T) \tag{2.12}$$

$$\nu_T = C_{NU}\frac{k^2}{\varepsilon} \tag{2.13}$$

Where k is the turbulent kinetic energy (TKE), P_T represents the turbulent kinetic energy production due to shearing effects, ε denotes the turbulent energy dissipation rate, and $Diff_k$ and $Diff_\varepsilon$ refer to the diffusion of TKE and dissipation, respectively. Additionally, C_{NU} and C_{DIS1} are dimensionless turbulence parameters with values of 1.42 and 0.085, respectively, while C_{DIS2}, another dimensionless turbulence parameter, is calculated from the k and P_T terms. The term μ

signifies the molecular dynamic viscosity, ν_T represents the turbulent kinematic viscosity, and ν_k and ν_ε denote the diffusion coefficients of k and ε, respectively.

For the model mesh, a staggered grid arrangement is used where all variables, such as pressures, fluid fractions, densities, turbulence quantities, and viscosities, are located at the center of the cells, except for velocities, which are located at the cell faces. This arrangement allows for efficient computational simulation of the fluid flow in the rock ramp fishway. The numerical solution advances through a time increment, denoted as δt, and involves three key steps. Firstly, explicit approximations of the momentum equations are employed to compute initial estimates for velocities at the next time step. These initial estimates account for various accelerations, such as advection, pressure, and other accelerations, using either initial conditions or values from the previous time step. Secondly, to satisfy the continuity equation, the pressures are iteratively adjusted within each cell. The velocity changes resulting from each pressure adjustment are then added to the velocities computed in the first step. This iterative process is necessary because changing the pressure in one cell can disrupt the balance in the neighboring six cells. Lastly, if a free surface or fluid interface is present, the free surface must be updated to reflect the new fluid configuration using a specific equation. By repeating these steps, the solution advances through the desired time interval. It is essential to note that at each of these steps, appropriate boundary conditions must be enforced at all mesh, obstacle, and free surfaces to maintain the integrity and accuracy of the simulations.

Methods

Model Development and Design

The numerical model was designed to replicate the experimental study carried out by Swarr (2018) at Colorado State University Foothills Fisheries Laboratory (CSU FFL) of a rock ramp fishway installed in a rectangular flume. The geometries were created using the dimensions provided by Swarr (2018). It consisted of a trapezoidal fishway with 30° side slopes and a 0.61 m base width, see Figure 2.1. The fishway is 6.1 m in length and 0.6 m in height. The fishway was installed in a 9.1 m x 1.2 m x 0.6 m flume.

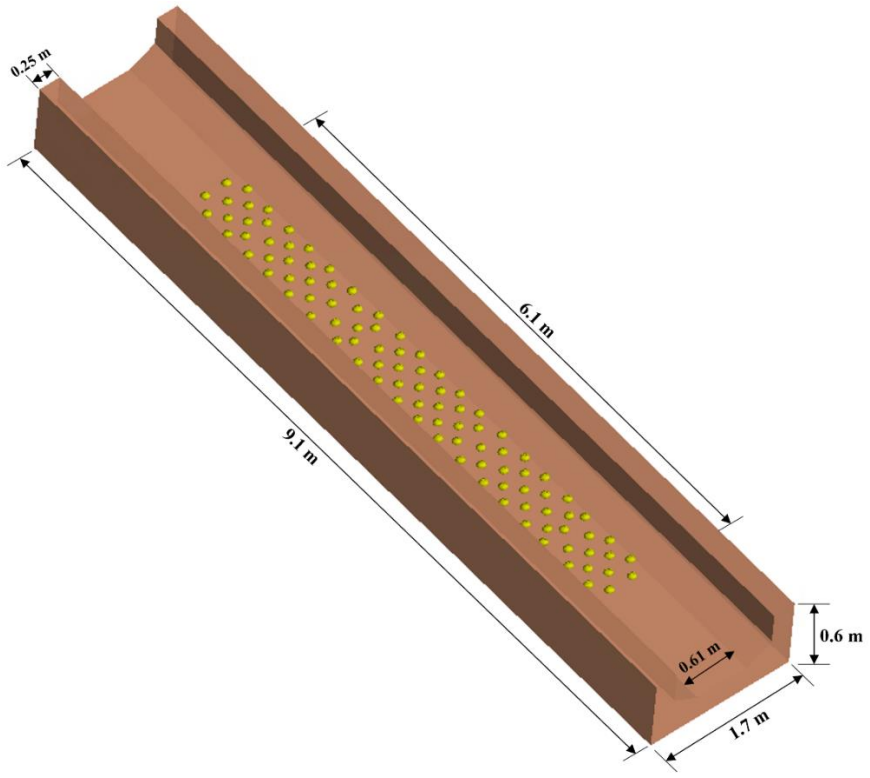


Figure 2.1: The flume and fishway geometry dimensions.

The model flume and fishway geometries were digitized in AutoCAD (Autodesk, 2023) using 3-D solids, with a wall thickness of 0.25 m for the model channel walls. The geometry was then exported as a stereolithography (.stl) file. Geometries in .stl format are well-supported and widely used in CFD software, including Flow-3D Hydro. The roughness elements used in the physical study were roughly hemispherical polyethylene rocks that are approximately 55 mm high and 95 mm in diameter. One of these rocks was scanned at the Montana State University Computer Integrated Manufacturing Laboratory using an Artec Space Spider 3D Scanner, see Figure 2.2. They were arranged in a staggered pattern throughout the length of the fishway. The rocks were placed in 39 rows, alternating between two and three rocks per row. The rock geometry was also exported as a .stl file, as shown in Figure 2.3. The 3D geometries were then imported into Flow-3D Hydro as solid impermeable objects, with the roughness elements placed at locations specified in the experimental study.

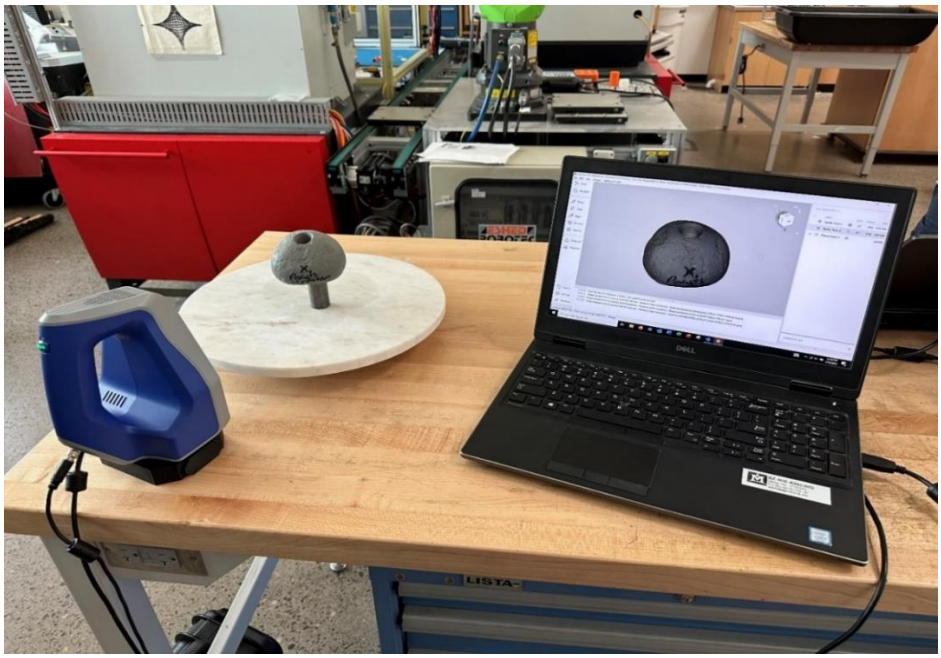


Figure 2.2: The rock being scanned with the Artec Space Spider 3D Scanner.

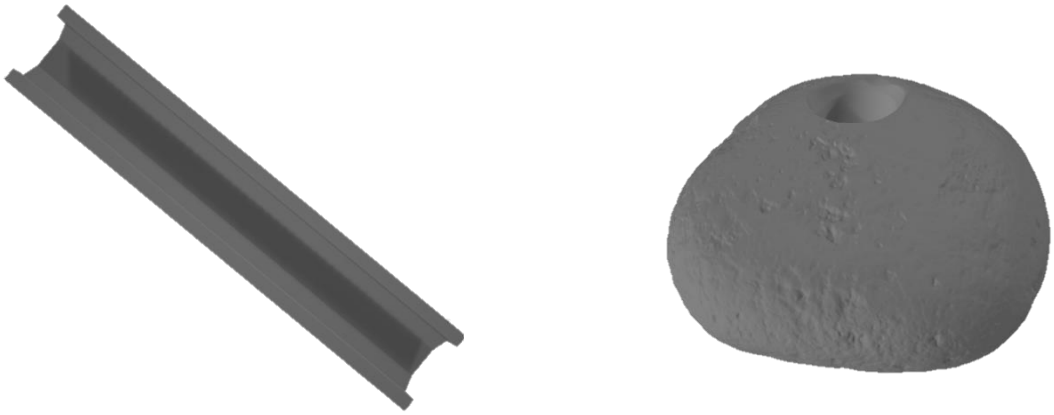


Figure 2.3: The fishway (left) and rock (right) 3-D STL geometries.

A computational mesh in a Cartesian coordinate system was created to define the simulation domain. The flume, fishway, and rock geometries were integrated into the mesh using the FAVOR method by partially obstructing the volumes and face areas of the cells. This means that the solid objects were inserted into the mesh without having to conform to it. As a result, the mesh and the rock ramp fishway geometries were defined independently. Flow-3D Hydro uses an orthogonal mesh structure where the grid lines are aligned with the coordinate axes, resulting in rectangular cells. For efficient meshing, multi-block meshing was utilized. Multi-block meshing involves dividing the computational domain into multiple mesh blocks, with each mesh block having its own unique mesh resolution. Since the areas around the rocks were of importance for this study, finer resolution mesh blocks were created for that region. These new mesh blocks were contained (nested) within the main mesh block. The advantage of the nested mesh block was that it enabled the areas around the rocks to be resolved with higher accuracy and fewer cells than using a single mesh block with fine resolution. Two types of nested mesh blocks were utilized for the study: non-conforming and conforming meshes. The non-conforming mesh block was finer than the containing mesh but coarser than the conforming mesh. The

higher resolution conforming mesh block was created to conform to the rocks. Conforming meshes are useful when there is a need to accurately capture a very thin solid region surrounded by fluid. The conforming mesh block accurately captured the surface of the rocks, while the non-conforming mesh block captured the behavior of the surrounding fluid. A total of three mesh blocks of varying resolutions, as shown in Figure 2.4, were used for each simulation in this study, and a size ratio of 2:1 between two adjacent mesh blocks was maintained. The ratio was used because it is the acceptable maximum ratio for multi-block meshing in Flow-3D Hydro to avoid significant inter-block accuracy loss. Mesh planes were introduced at all interfaces joining the mesh blocks to help with the grid alignment. Mesh planes were aligned with the edges of the nested mesh blocks. This approach ensured the most efficient and accurate exchange of data between the mesh blocks.

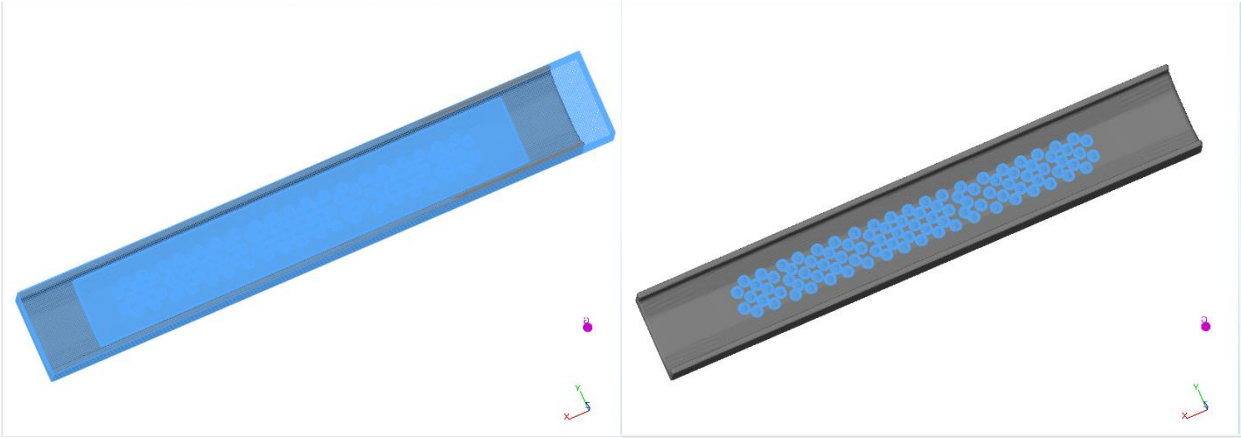


Figure 2.4: The three mesh blocks used for the fishway (left) and the conforming mesh (right).

The equations governing the motion of fluid flow require descriptions of the initial conditions and the boundary conditions to find a solution. The boundary conditions define the behavior of the fluid flow at the mesh boundaries. Boundary conditions were applied to all

exterior planes, defining the computational mesh regions of this study. Swarr (2018) focused on identifying the ideal slope for rock ramp fishways to successfully pass a variety of small-bodied Great Plains fish. The authors examined five different slopes with flows set at five different flow rates to maintain a flow depth of approximately 51 mm at each slope, see Table 2.1.

Table 2.1: Slopes and their respective flow rates used in the experimental study.

Slopes (%)	**Flow Rates (m^3/s)**
2	0.00743
4	0.00963
6	0.0229
8	0.0316
10	0.0363

Since the flow rates were known, the upstream boundary condition was set to *Volume Flow Rate*. This condition applied the specified flow rates for each slope at the upstream mesh boundary. As a boundary condition of the Dirichlet type, where fluid crosses the boundary, it was necessary to specify how the fluid would be distributed along the mesh face. The fluid elevation was selected as the parameter to define the free surface. This elevation was adjusted to ensure that the flow depth at that boundary remains at approximately 51 mm. Below the specified fluid elevation, it is transformed into a fluid fraction of $F = 1$, while above the designated fluid elevation, it becomes $F = 0$. A *Pressure* boundary condition was applied at the downstream and the top boundaries. The fluid elevation was set at the downstream boundary to replicate the experimental tailwater depth, which is 51 mm. A fluid fraction of zero was selected for the top boundary condition. This boundary condition type will remove any fluid that touches the top domain. The bottom and the sides of the computational domain were defined as *Wall* boundaries.

These boundaries were completely blocked by the solid objects, and they act like hydraulically smooth no-slip surfaces. There was no interaction between these boundaries and the fluid, hence they had little or no effect on the model. These boundaries were applied to the containing (outer) mesh block. For the nested mesh blocks, *Symmetry* boundary conditions were applied to all the mesh boundaries. The boundary conditions for the rock domain were not significantly relevant, as the mesh blocks were contained inside the outer mesh block. In Flow-3D Hydro, the preprocessor assigns these interior boundaries as inter-block type boundaries, ensuring consistency and coherence within the mesh. These inter-block boundaries are only used to interpolate the data between adjacent mesh blocks. In other words, the *Symmetry* boundary conditions for the nested meshes were overridden by the preprocessor.

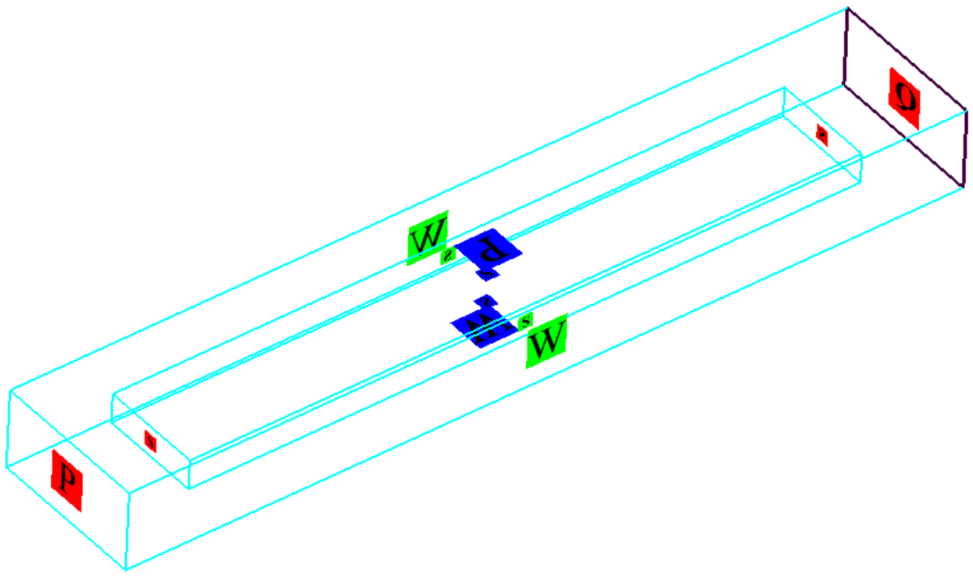


Figure 2.5: The boundary conditions for the three mesh blocks.

Table 2.2: Summary of the boundary conditions.

Boundary	**Fishway Mesh**	**Rock Mesh (Non-conforming)**	**Rock Mesh (Conforming)**
X - min	Volume Flow Rate (**Q**)	Symmetry (**S**)	Symmetry (**S**)
X - max	Pressure (**P**)	Symmetry (**S**)	Symmetry (**S**)
Y - min	Wall (**W**)	Symmetry (**S**)	Symmetry (**S**)
Y - max	Wall (**W**)	Symmetry (**S**)	Symmetry (**S**)
Z - min	Wall (**W**)	Symmetry (**S**)	Symmetry (**S**)
Z - max	Pressure (**P**)	Symmetry (**S**)	Symmetry (**S**)

The initial conditions of the model describe the conditions of the fluid flow at t=0. Beginning the simulation with an empty flume resulted in long model run times as the flume needed to fill with water and then reach a steady state. A fluid region was created to fill the flume at a constant depth of 51 mm to reduce the run time. This implied that the simulation would start with a flume containing water at t = 0. An initial velocity of zero m/s was assigned to the fluid region. The creation of the fluid region involved utilizing Flow-3D Hydro primitive geometries, which are simple shapes used to define objects. The fluid region was inclined at different angles corresponding to each slope.

The fluid was defined as water with a density of 998.2 kg/m^3 and a dynamic viscosity of 0.001 Pa-s (kg/m-s). The water temperature was specified as 20°C, corresponding to the physical experiment's water temperature. Additional physical models were activated within the software. For this study, the gravity model was activated, as well as the turbulence and viscosity models. Gravity was defined as acting in the negative z-direction with a magnitude of 9.81 m/s^2. Furthermore, the wall shear boundary condition was defined within the turbulence model. The

dynamically computed maximum turbulent mixing length option was selected. Turbulent mixing length represents the characteristic length scale that corresponds to the size of the smallest turbulent eddy that will be resolved within a fluid flow. Eddies smaller than this length were not resolved but were approximated within a mean quantity. This implies their effects were included in the simulation, but their individual behavior was not explicitly resolved. The maximum turbulent mixing length served as an upper stability threshold to prevent overestimation of the length scale of turbulence by the turbulence model. Since the *Dynamically Computed* option was selected, the maximum turbulent mixing length was automatically computed during the simulations based on time and location.

Before initiating the simulations, the numerical options for governing equation discretization and control were specified. A second-order monotonicity preserving scheme was implemented for the momentum advection to accurately capture secondary flows within the fishway. This method approximated the momentum advection, density, and fluid fraction advection in a second-order accurate manner in space and first-order accurate in time. The default techniques for the advection of momentum and all other fluid quantities are based on explicit numerical approximations. Explicit methods are simple and accurate but require a limit on the maximum time-step size to maintain numerical stability. The explicit advection solver option resulted in time-step limitations due to convection for the simulations, which led to software warnings. To fix the warning, an implicit numerical solver option was selected. This implicit solver option removed the limitation on the maximum time-step size required for numerical stability. An explicit/implicit velocity threshold was selected, and a velocity threshold of 5 m/s was specified. Ideally, the velocity threshold should be set to a value larger than the

velocity of the bulk of the fluid and smaller than the velocity of the fast droplets. In the earlier simulation setup that led to the software warnings, the velocities in the bulk of fluid were not greater than 5 m/s. For that reason, this specific value was selected. With this setting, the advection terms are evaluated explicitly for cells with velocities below the specified threshold and implicitly for cells with velocities above the threshold. Generally, the default numerical settings were used unless unsatisfactory results or software warnings or suggestions indicated otherwise.

The finish conditions were defined prior to the simulation initiation. These conditions refer to the criteria that determine when a simulation should stop under normal conditions. A finish time and a steady-state condition were specified. The steady-state conditions were deemed to be achieved when there was a maximum allowable deviation of one percent in the average mean kinetic energy, the average mean turbulent energy, the average mean turbulent dissipation, and the total mass. The simulations terminated at the specified finish time or when the established steady-state conditions were met. When the specified finish time was reached without meeting the one percent maximum variation threshold, further analysis was conducted to assess the convergence of the simulations affected. These convergence analyses involved evaluating both the maximum variation threshold and the mean stationarity for the variables of interest. The maximum variation threshold assesses if the change in the value of the variables from one iteration to the next drops below a set tolerance, while the mean stationarity assesses if the average value of the variables stops changing between iterations. The variables considered for the convergence proof were the mean kinetic energy and average turbulent energy. These variables were assessed for the maximum variation threshold and stationarity to determine

whether a satisfactory convergence was achieved. All simulations either met the steady state conditions or the convergence analysis.

Mesh Independence Study

Generally, it is known that as the mesh is refined, the numerical error decreases, leading to a more accurate solution. However, those mesh refinements also increase the computational cost. Therefore, there is a need to find a compromise between accuracy and performance. The goal of this 3-D mesh independence analysis was to identify the minimum mesh resolution required to achieve sufficiently accurate and converged results for the numerical simulations without excessive computational cost. The analysis was performed on the 2% slope fishway. Using the lowest slope with the lowest flow rate is an effective way to ensure that the mesh captures the smallest flow feature accurately. Simulations with six different mesh sets, as illustrated in Table 1, were created to examine the mesh independence solution for the simulation of the rock ramp fishway. To save time and reduce the computational cost, the mesh was not refined beyond Mesh 6. Further refinement would lead to a large total number of cells, making the simulation computationally expensive. Each mesh set included the mesh sizes for the outer and the two nested mesh blocks. The size differences between the mesh blocks in each mesh set were maintained at a 2 to 1 ratio for accuracy. The RNG k-ε turbulence closure model was utilized.

Table 2.3: Summary of the grid sizes.

	Outer Mesh Size (m)	**Non-conforming Mesh Size (m)**	**Conforming Mesh Size (m)**	**Total Number of Cells**
Mesh 1	0.08	0.04	0.02	610,790
Mesh 2	0.07	0.035	0.0175	922,716
Mesh 3	0.06	0.03	0.015	1,429,780
Mesh 4	0.05	0.025	0.0125	2,504,448
Mesh 5	0.04	0.02	0.01	4,895,700
Mesh 6	0.03	0.015	0.0075	11,537,176

The free surface elevation (also known as water surface elevation) was used to show how sensitive the simulation solutions are to grid sizes. The free surface elevation gives global, integral insight into the fishway hydraulics and flow physics. Fifteen (15) data points spread throughout the fishway were chosen for the investigation. The root mean square error (RMSE) between consecutive mesh sizes was calculated and plotted to visualize the convergence of the results as the mesh becomes finer. The RMSE was calculated using:

$$RMSE = \sqrt{\frac{\sum_{i=1}^{N}(M_i - S_i)^2}{N}} \tag{2.14}$$

Where M_i and S_i are the measured and simulated results, respectively, and N is the total number of data points. The RMSE of the free surface elevations for the different mesh sizes were plotted in Figure 2.6.

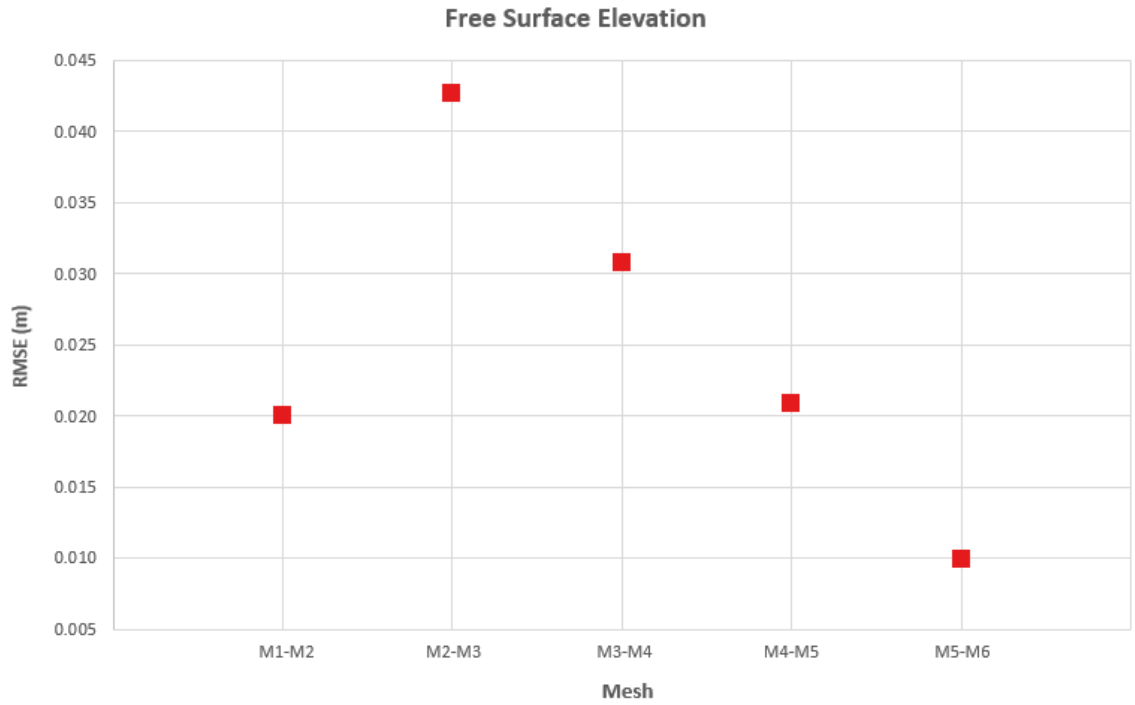


Figure 2.6: The RMSE plot for the different mesh sizes.

The findings obtained, as shown in Figure 2.6, showed that the different mesh sizes had a significant influence on the free surface elevation. The RMSE between Mesh 1 and Mesh 2 seemed small but when the mesh size was made finer, the error increased. Thereafter, the error began decreasing as the mesh became finer. It was observed that Mesh 5 and Mesh 6, which represented the finest meshes utilized in the study, exhibited similar outcomes. The RMSE is calculated as 0.01 m, indicating a small difference between the two models. This convergence suggested that further refinement of the mesh beyond Mesh 6 would yield negligible improvements in terms of accuracy. These observations indicated that the simulations had achieved a level of mesh independence. Consequently, to achieve optimal computational efficiency while preserving accuracy, Mesh 6 was selected over Mesh 5 as the most suitable mesh size for subsequent numerical simulations. There is potentially more accuracy and

resolution in representing the geometry and capturing flows within the rock ramp fishway using Mesh 6. This selection effectively balances the trade-off between accuracy and computational resources.

Sensitivity Test

Numerical simulations may be affected by various input parameters. Therefore, sensitivity analysis of the simulation is required. A sensitivity analysis was conducted to explore how uncertainties or changes in input parameters affect the output results of the numerical simulations. The input parameters investigated in this uncertainty analysis were the turbulence model and the roughness height. Free surface elevation was selected as the output parameter. The input variables were varied to determine their effect on the free surface elevation. Mesh 6 was utilized for the sensitivity test. Furthermore, the 2% slope fishway was used for the analyses, and the flow rate specified at the inflow boundary was 0.00743 m^3/s.

Turbulence model: Turbulence models are approximations. Different turbulence models make different simplifying assumptions about the physics of turbulent flows. Testing the different models can show the sensitivity of the simulation results to the choice of turbulence model. Flow-3D Hydro has four turbulence models for 3D simulations: Large Eddy Simulation (LES), the two-equation k-omega (k-ω), standard k-epsilon (k-ε), and Renormalized Group (RNG) k-ε. Of these four, the three two-equation Reynolds-Averaged Navier-Stokes (RANS) models were selected for the analysis. The LES model was omitted because it is computationally much more expensive than the two-equation models. It also requires a well-refined mesh and takes a long time to converge. Three different simulations were performed with a different turbulence model for each simulation. While the turbulence model was varied, other conditions

and parameters were kept constant. The roughness height for the fishway was maintained at 0.0015 mm throughout the turbulence model sensitivity test. A finish time and steady-state termination conditions were prescribed.

The results of the effect of the different turbulence models on the free surface elevation are graphically illustrated in Figure 2.7. As shown in Figure 2.7, the free surface elevation did not significantly change with changes in the turbulence model used for the simulation. As a result, the default turbulence model, the RNG k-ε, was utilized for all the simulations in this study.

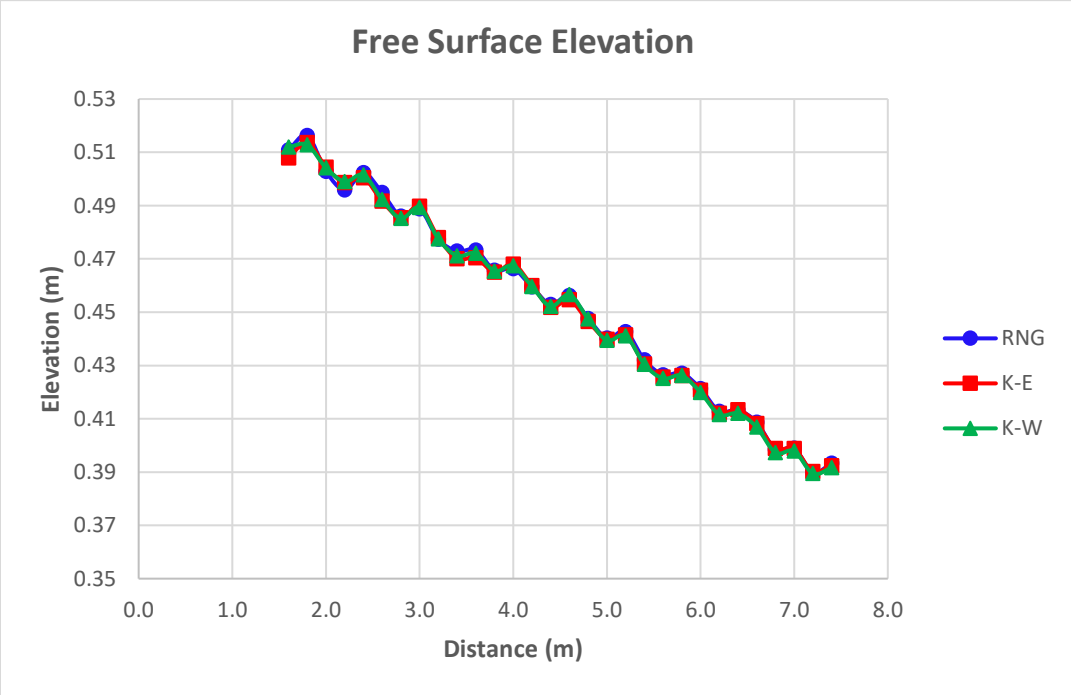


Figure 2.7: Plot of the free surface elevation along the longitudinal centerline for the turbulence models.

Roughness: Roughness height refers to the average height of the surface irregularities of an object or a geometry. Appropriate roughness height specification is critical for accurately

predicting wall shear stress, velocity profiles, boundary layer thickness, and turbulence production in the near-wall region. The fishway was constructed from polyvinyl chloride (PVC) sheets, while the rocks in the structure were fabricated using polyethylene (PE) (Swarr, 2018). The roughness heights for PVC and PE typically range from 0.0015 mm to 0.007 mm (The Engineering ToolBox, 2003). Three simulations were conducted to assess the influence of the varying roughness heights associated with the PVC sheet and the PE rocks on the flow behavior within the fishway. For each simulation, the same roughness heights were applied to both the fishway and the rocks. The roughness heights of 0.0015 mm, 0.00425 mm, and 0.007 mm, representing the lower, middle, and upper bounds within the roughness height range, were evaluated.

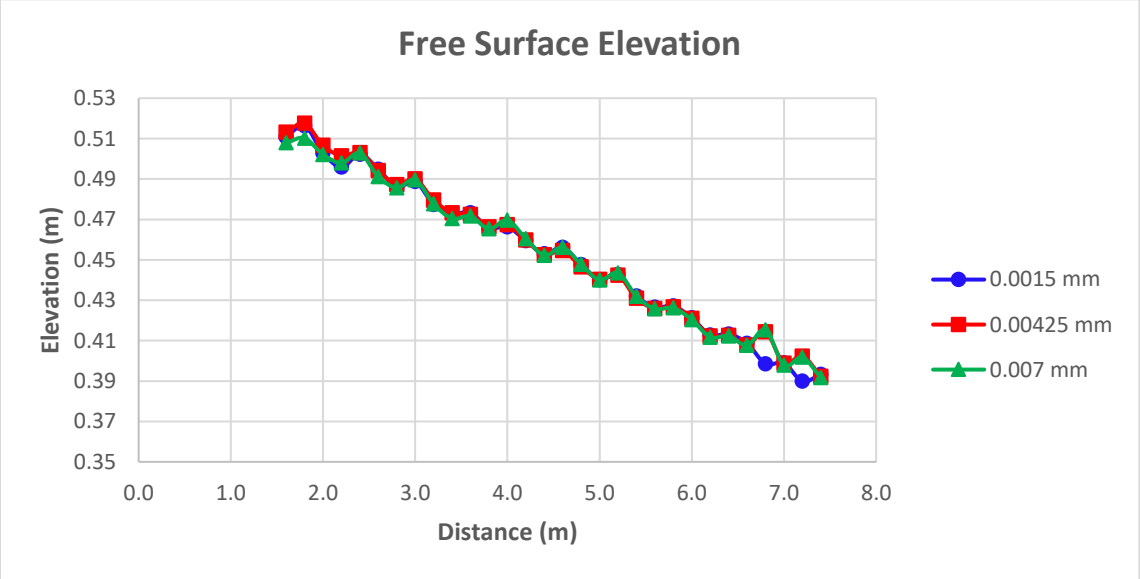


Figure 2.8: Plot of the free surface elevation along the longitudinal centerline for the roughness heights.

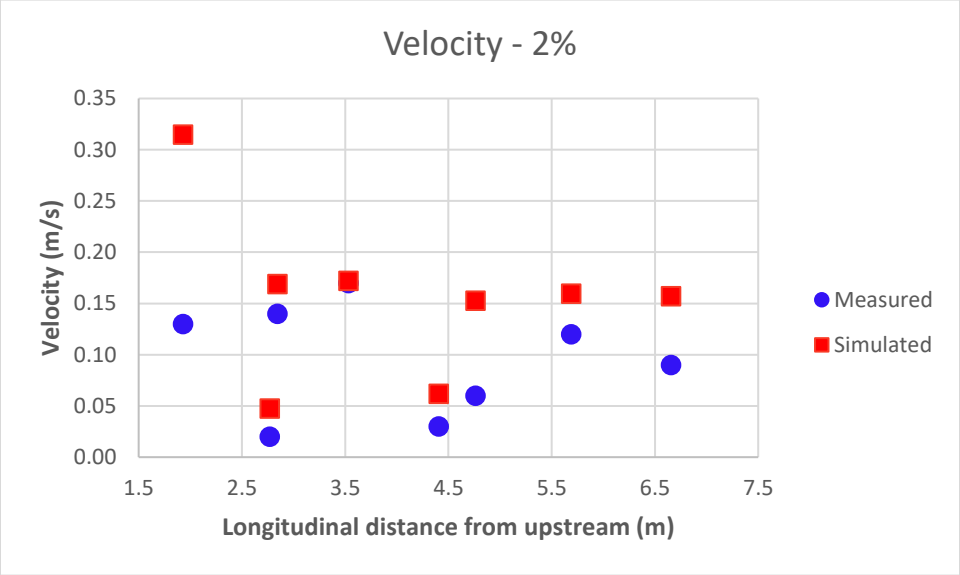
As illustrated in Figure 2.8, the results indicated that the variation in roughness heights had minimal impact on the free surface elevation solution. Therefore, a roughness height of 0.0015 mm was considered for further investigations within the fishway.

Model Validation

Simulations of all slopes and corresponding flow rates examined in the experimental study by Swarr (2018) were completed. To assess the ability of the numerical model to replicate the hydrodynamics of the rock ramp fishway flow and validate model accuracy, the numerical results were compared with the measurements obtained from the physical experiments. Depth-averaged velocity and flow depth were used for data comparison as both variables have been measured and recorded in the physical experiments. The depth-averaged velocity refers to the average velocity of the fluid over its entire depth, calculated by taking the magnitude of the velocity and averaging it over the vertical column. Flow depth, on the other hand, represents the vertical distance from the free surface of the fluid to the channel bed. The measured and simulated results were compared for the 2% and 10% slopes. The slopes denote the mildest slope with the lowest flow rate and the steepest slope with the highest flow rate, respectively. These slopes represent the extremes of the range of slopes and flow rates. Data obtained from these two slopes encompassed the entire spectrum of slopes and flow rates utilized in the study. The agreement between the physical experiments and the simulations was quantified using RMSE. Additionally, a paired t-test was conducted to compare the mean values of the measured and simulated parameters. The alternative hypothesis was that there was a difference between the physical and numerical models. The significance level for this test was set at 0.05 to determine if the observed difference was statistically significant. Results from two transects of the fishway,

the longitudinal centerline and a cross-section located halfway down the fishway, were compared for validation.

Velocity: The velocity for each numerical simulation was compared to the velocity obtained in the physical experiment carried out by Swarr (2018). In the physical model, the velocities were measured at approximately 0.6H from the water surface, with H representing the total flow depth at a specific section. A Marsh McBirney flowmeter was used for these measurements (Swarr, 2018). The velocities obtained through the laboratory measurements and the numerical simulations are illustrated in Figures 2.9 and 2.10. The RMSE between the measured and simulated velocities from the streamwise centerline of the fishway was 0.080 m/s for the 2% slope and 0.310 m/s for the 10% slope. For the cross-section, the RMSE for the 2% and 10% slopes were calculated as 0.099 m/s and 0.171 m/s, respectively. A statistically significant difference in mean velocity was observed for the 2% slope ($p = 0.023$) for the streamwise centerline. However, there is no evidence to suggest that there is a difference in the mean velocity for the 10% slope for both transects and for the predicted values obtained in the cross-section in the 2% slope, as indicated by the p-value in Tables 2.4 and 2.5. The CFD models overestimated most of the velocities in the 2% slope while underestimating them in the 10% slope.



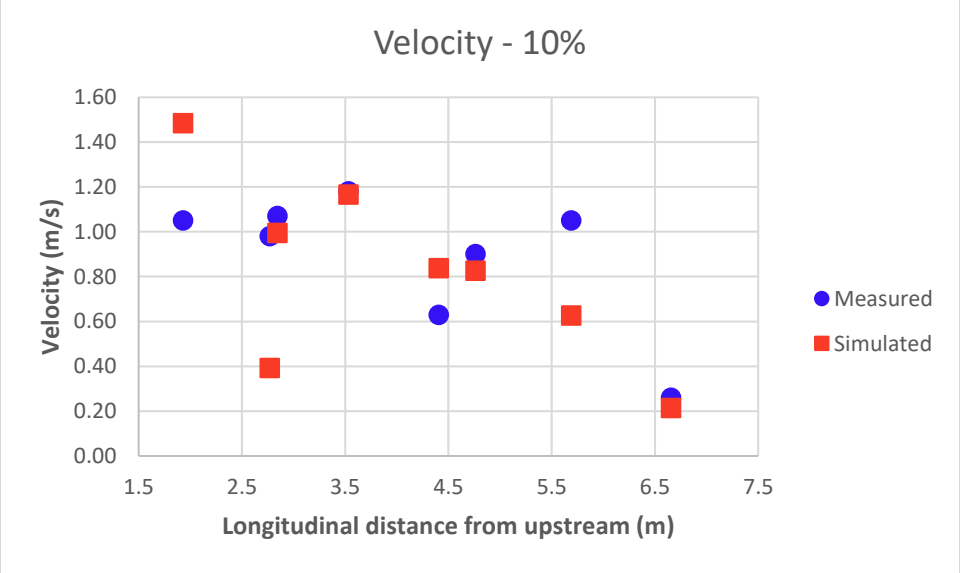


Figure 2.9: Velocities comparison between the simulated and the measured values at the 2% and 10% slopes along the streamwise centerline.

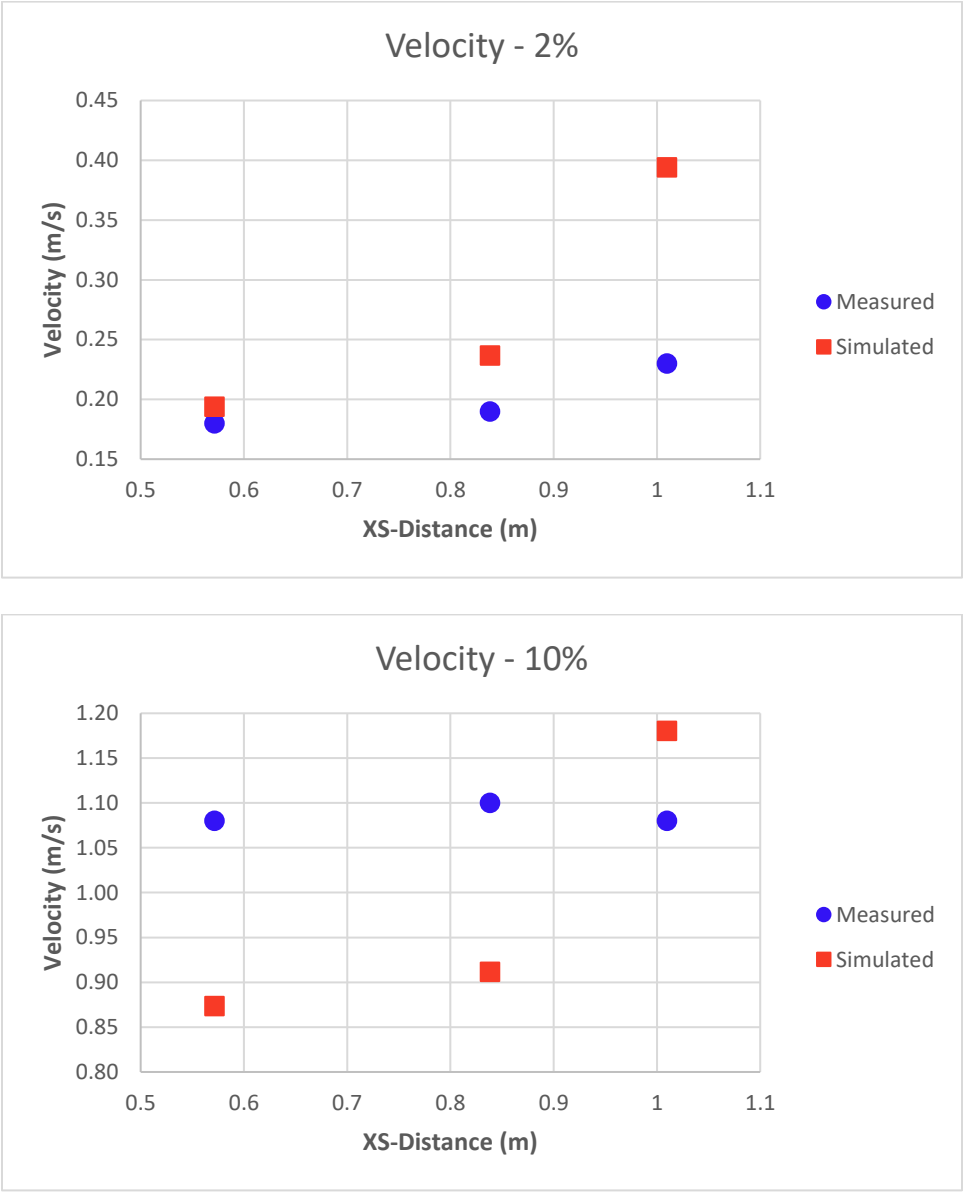


Figure 2.10: Velocities comparison between the simulated and the measured values at the 2% and 10% slopes along the mid cross-section.

Several factors may contribute to discrepancies between modeled and observed velocities. Firstly, the CFD models provided depth-averaged velocities. The velocity at 0.6H from the surface is typically lower than the depth-averaged velocity. While not an exact equal comparison, the depth-averaged velocity can provide a reasonable upper bound estimate for the

0.6H velocity. Secondly, the numerical model utilized an idealized representation of the geometry of the rock ramp fishway used in the physical experiment. It does not account for any imperfections or deviations present in the physical model. Thirdly, inaccuracies in the calibration of either the flowmeter or the CFD model can impact the velocities at specific points. Lastly, accurately measuring velocities in very shallow flows near the bed can be challenging with standard instrumentation. Additionally, insufficient grid resolution near the bed and around the rocks in the numerical model can result in a poor representation of the velocity.

Although there were disparities between the measured and simulated velocities, the numerical model successfully captured the velocity pattern of the physical model, as depicted in Figures 2.9 and 2.10. Additionally, the CFD model produced velocity values that closely aligned with the measurements from the physical study. This similarity was confirmed statistically, with p-values exceeding 0.05.

Flow depth: The simulated water depths were also compared with observations from the physical model. At the centerline of the fishway, the RMSE between the observed and simulated flow depths was 0.0066 m and 0.0341 m for the 2% and 10% slopes, respectively. The errors were 0.0037 m and 0.0147 m for the respective slopes for the cross-section of the fishway. The t-test indicated no significant differences in the mean depths of the physical and numerical models for the slopes and transects, except for the 2% slope in the centerline measurement. The centerline depth of the 2% slope showed a significant difference with a p-value of 0.014. On the other hand, the cross-section measurements for the same slope did not reflect a substantial discrepancy with a p-value of 0.125. Similarly, measurements on the 10% slope did not show any significant difference either, depicted by the p-values of 0.164 (centerline) and 0.402 (cross-

section) respectively. As illustrated in Figures 2.11 and 2.12, the flow depths were under-predicted by the numerical models.

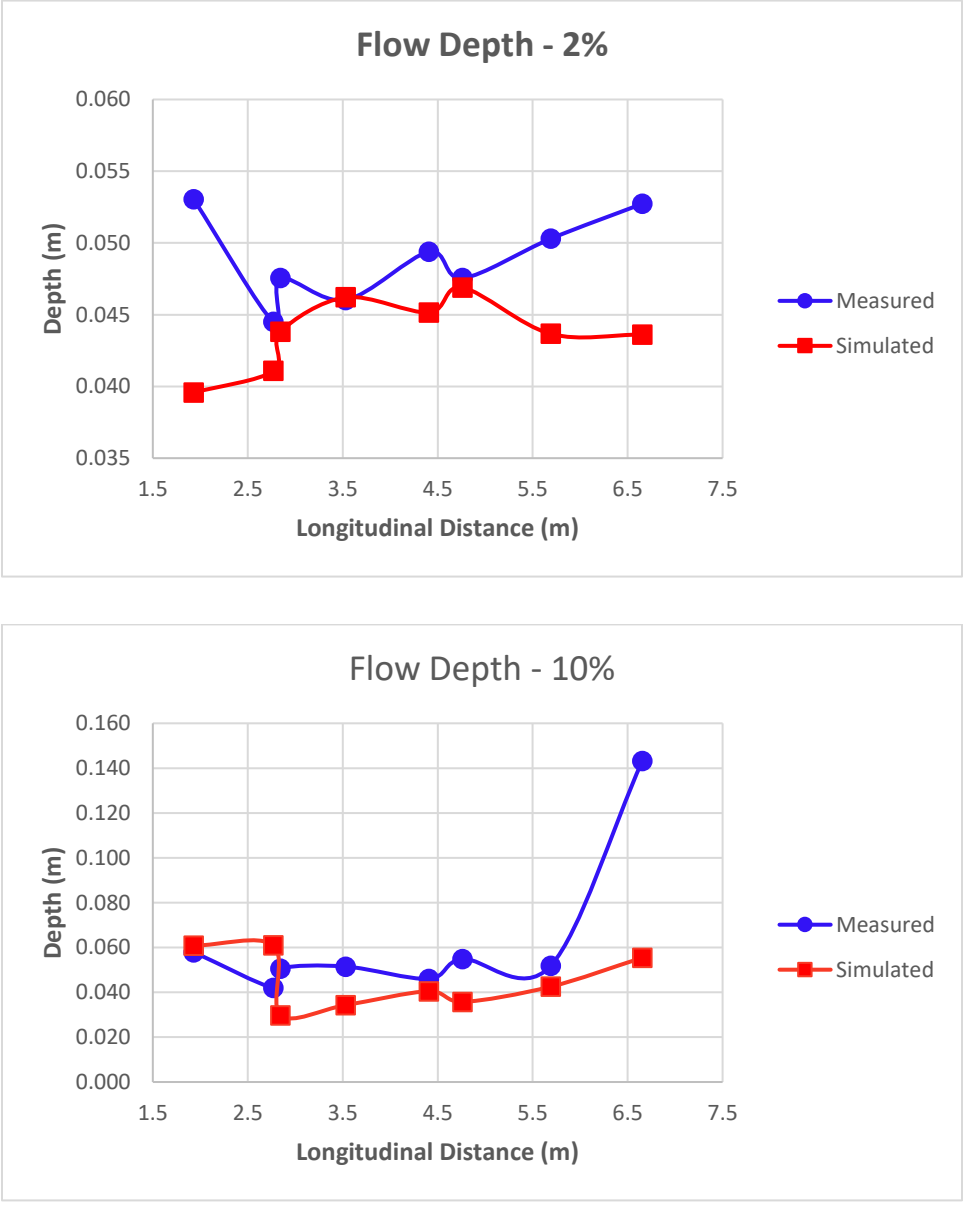


Figure 2.11: Water depth comparison between the simulated and the measured values at the 2% and 10% slopes along the streamwise centerline.

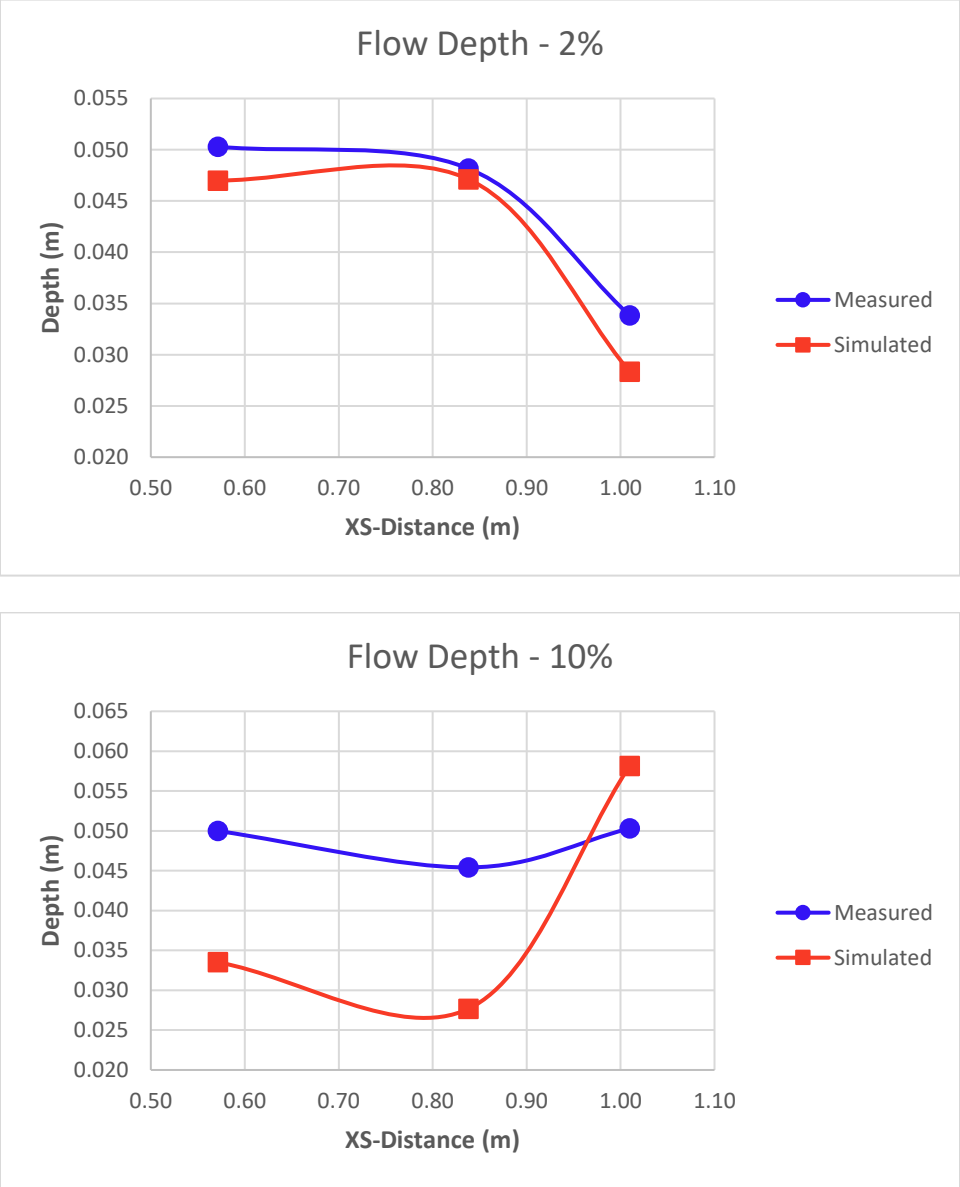


Figure 2.12: Water depth comparison between the simulated and the measured values at the 2% and 10% slopes along the mid cross-section.

The under-prediction of the flow depths by the numerical models may be attributed to several factors. Uncertainties in the physical model measurements can impact the validation process. Despite rigorous efforts to obtain accurate measurements, there can be inherent errors or variations in the experimental data. These uncertainties can affect the comparison between the

measured and simulated flow depths, potentially leading to discrepancies. Additionally, simplifications and assumptions made in the numerical model can also influence the accuracy of the predictions. Assumptions about boundary conditions or other simplifications, although necessary, can introduce some level of discrepancy between the simulated and physical models. The predicted flow depths show generally good agreement with the experimental data. As seen in Figures 2.11 and 2.12, similar patterns were also observed between the measured and simulated flow depths.

The comparison of measured and simulated velocity and flow depth results in the rock ramp fishway study was summarized in Table 1. This comparison indicated both successes and challenges in the numerical modeling approach. Despite the observed differences, the numerical model successfully captured the overall flow patterns observed in the physical model. A smaller RMSE generally indicates a higher level of agreement between the model predictions and the actual measurements. In this study, the CFD model demonstrated relatively low errors, indicating good accuracy in predicting the flow depth and velocity. With generally good agreement between the simulated and experimental data, the numerical model demonstrated the ability to provide a reasonable representation of the flow behavior in the rock ramp fishway. Furthermore, the similarity in patterns between the predicted and measured flow depths further emphasized the capability of the numerical model to accurately estimate the flow characteristics in real-world scenarios. Considering the overall quality of the numerical model results, it was determined that the numerical model is adequate for simulating the flow characteristics in the rock ramp fishway.

Table 2.4: Summary of the results of the model validation measured along the centerline.

Slopes (%)	Observed Mean Velocity (m/s)	Simulated Mean Velocity (m/s)	$RMSE_{vel}$ (m/s)	Velocity p-value	Observed Mean Flow Depth (m)	Simulated Mean Flow Depth (m)	$RMSE_{depth}$ (m)	Depth p-value
2	0.0950	0.1543	0.0801	0.0230	0.0489	0.0438	0.0066	0.0140
10	0.8900	0.8180	0.3101	0.547	0.0623	0.0450	0.0341	0.1640

Table 2.5: Summary of the results of the model validation measured along the mid cross section.

Slopes (%)	Observed Mean Velocity (m/s)	Simulated Mean Velocity (m/s)	$RMSE_{vel}$ (m/s)	Velocity p-value	Observed Mean Flow Depth (m)	Simulated Mean Flow Depth (m)	$RMSE_{depth}$ (m)	Depth p-value
2	0.2000	0.2749	0.0988	0.2420	0.0441	0.0408	0.0037	0.1250
10	1.0867	0.9884	0.1714	0.4270	0.0486	0.0398	0.0147	0.4020

Results and Discussion

To examine the rock ramp fishway, the study evaluated the flow depth, the flow velocity, and the turbulent kinetic energy. These parameters were selected as they constitute the primary hydraulic attributes of an open channel (Cao et al., 2020; Zheng et al., 2020). The significance of these parameters lies in their direct impact on fish behavior, swimming capabilities, and the overall success of fish passage within the fishway (Bretón et al., 2013; Carrero-Díez et al., 2022). The simulation results, illustrating the maximum, median, minimum, and mean values of the studied flow parameters, are presented in Tables 2.6 to 2.8.

Table 2.6: Summary of the predicted values for the flow depths.

Slope (%)	Flow Rate (m^3/s)	Maximum Depth (m)	Median Depth (m)	Minimum Depth (m)	Mean Depth (m)
2	0.00743	0.0719	0.0518	0.0090	0.0510
4	0.00963	0.0729	0.0555	0.0082	0.0534
6	0.0229	0.0825	0.0579	0.0079	0.0554
8	0.0316	0.0913	0.0656	0.0087	0.0629
10	0.0363	0.0984	0.0703	0.0087	0.0679

Table 2.7: Summary of the predicted values for the flow velocities.

Slope (%)	Maximum Velocity (m/s)	Median Velocity (m/s)	Minimum Velocity (m/s)	Mean Velocity (m/s)
2	0.8164	0.2804	0.0000	0.2719
4	1.1524	0.4109	0.0000	0.3982
6	1.5829	0.6628	0.0000	0.6509
8	1.8027	0.8221	0.0000	0.8179
10	2.0751	0.9925	0.0000	1.0033

Table 2.8: Summary of the predicted values for the turbulence kinetic energy.

Slope (%)	Maximum TKE (J/kg)	Median TKE (J/kg)	Minimum TKE (J/kg)	Mean TKE (J/kg)
2	0.0526	0.0028	0.0000	0.0032
4	0.1633	0.0054	0.0000	0.0068
6	0.1945	0.0096	0.0000	0.0118
8	0.0912	0.0116	0.0000	0.0122
10	0.0769	0.0137	0.0000	0.0136

Flow Depth

The predicted longitudinal water depths along the centerline of the fishway were analyzed for the different slopes. The rectangle in Figure 2.13 indicates the area that was visualized. As depicted in Figure 2.14, it was observed that the water began to overtop the rocks with increasing slope and flow rates. The maximum water depth occurs immediately upstream of the rocks in the simulations. The rocks blocked some of the cross-section, which led to water backing up upstream of the rocks. Additionally, the water level drops in the wake downstream of the rocks. This water depth reduction in the wakes is attributed to the flow area expansion due to the diversion of the water flow around the rocks. This pattern was in agreement with the observations by Baki et al. (2014), Cassan et al. (2014), and Baki et al. (2016).

The flow depth in the wake decreased as the slope increased. As the bed slope increases, the flow velocity increases. With this heightened velocity, the water gains more kinetic energy as it moves downstream. The increased velocity and kinetic energy caused the flow to have less time to accumulate behind the rocks and form a deep wake. Therefore, the wake becomes shallower. At lower flows and milder slopes, the water moves more slowly and has less energy. The wake region becomes longer and deeper, as seen in Figure 2.14. The maximum flow depths decreased as the flow rates and slopes decreased, as can be seen in Table 2.6. The highest maximum flow depth, 0.0984 m, was observed with the maximum flow in the 10% slope. The location of the maximum depths was immediately upstream of the rocks.

Based on the results, the rock ramp fishway can create pools of water deep enough for fish to rest in. Increased water depths within the fishway facilitate a more conducive and less arduous migration process for small-bodied fish navigating upstream, reducing their overall fatigue risks (Shiau et al., 2020). The recommended minimum flow depth is 1.5 times the fish

body thickness (Maine Department of Transportation, 2004). Based on this recommendation, the minimum flow depths for Arkansas Darter, Stonecat, and Flathead Chub are approximately 0.02 m, 0.04 m, and 0.03 m, respectively. The mean depths for all the slope treatments exceeded the minimum required flow depths for the target species. However, the decreased flow depth at the wake can have a significant impact on the successful passage of the small-bodied fish. Fish typically use wakes as resting areas, where they can conserve energy. A shallow wake provides less resting space for fish, which can make it more difficult for them to pass through the fishway.

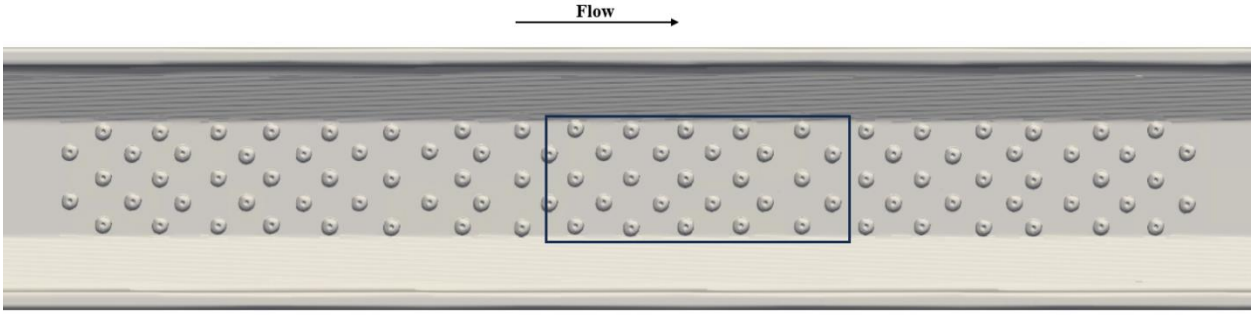


Figure 2.13: The model domain visualized for flow depths.

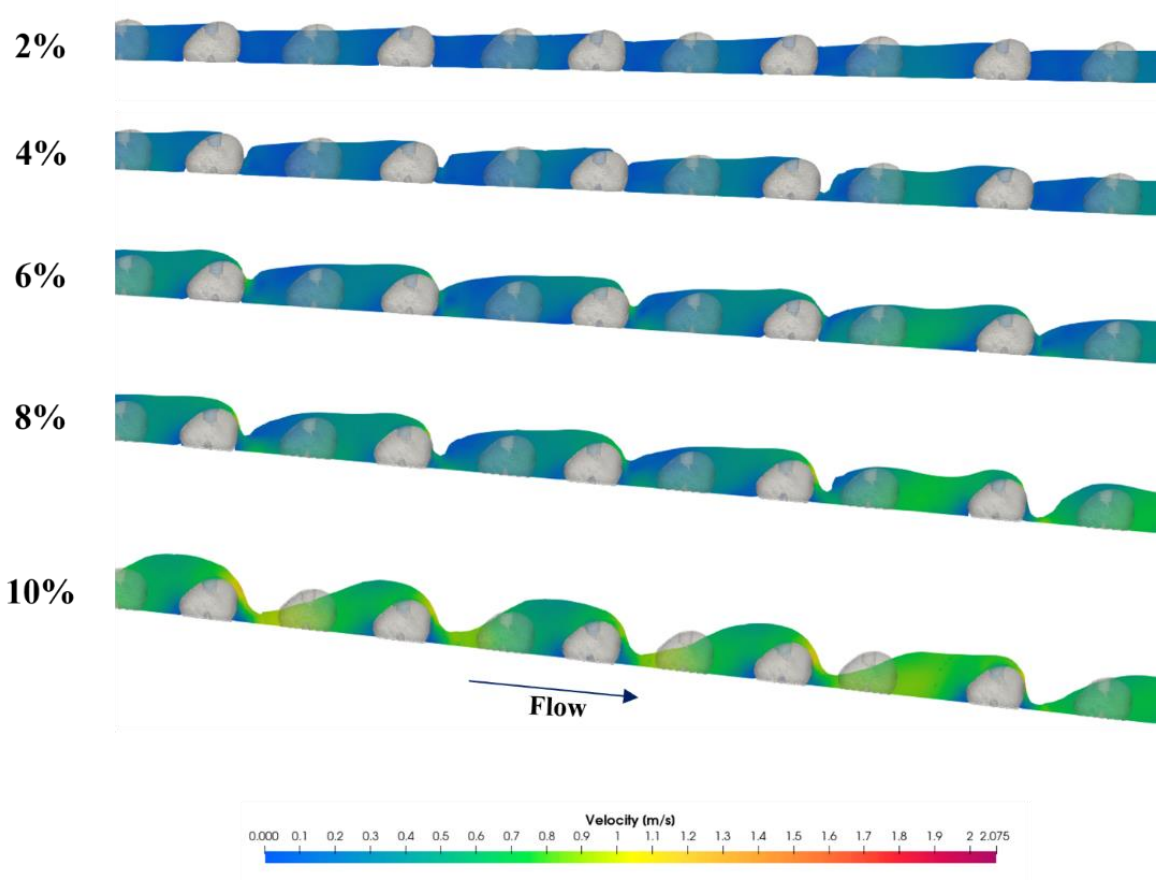


Figure 2.14: Longitudinal flow depths for the different slopes colored by velocity.

Velocity

The study demonstrated a direct correlation between slope, flow rate, and velocity. The results established that as slopes and flow rates increase, the velocity also increases. These findings are consistent with the conservation of momentum within the fluid stream under varying slope conditions and flow rates. Table 2.7 summarizes the predicted velocity for each slope. Distinct velocity distributions were observed in the fishway. The lowest velocities were observed in the wake region for all the slope treatments, as in Figure 2.15. Across the cross-section, as illustrated in Figures 2.18 to 2.21, it also illustrates that the wake region consistently displayed the lowest velocities, indicating unique flow behaviors behind the rocks. Immediate velocity

reductions were observed downstream of the rocks, accompanied by higher velocities on the sides of the rocks. This spatial variation illustrates complex flow patterns and suggests energy dissipation effects. The findings coincided with the observations made by Hockley et al. (2014) and Swarr (2018). The low-velocity zones in the wake of the rocks are important to the success of rock-ramp fishways. These zones occur when the rocks create turbulence, which slows down the water flow, thereby creating pockets of low velocity behind the rocks. Due to the low velocity in the wake, fish utilize it as a resting area while ascending the fishway.

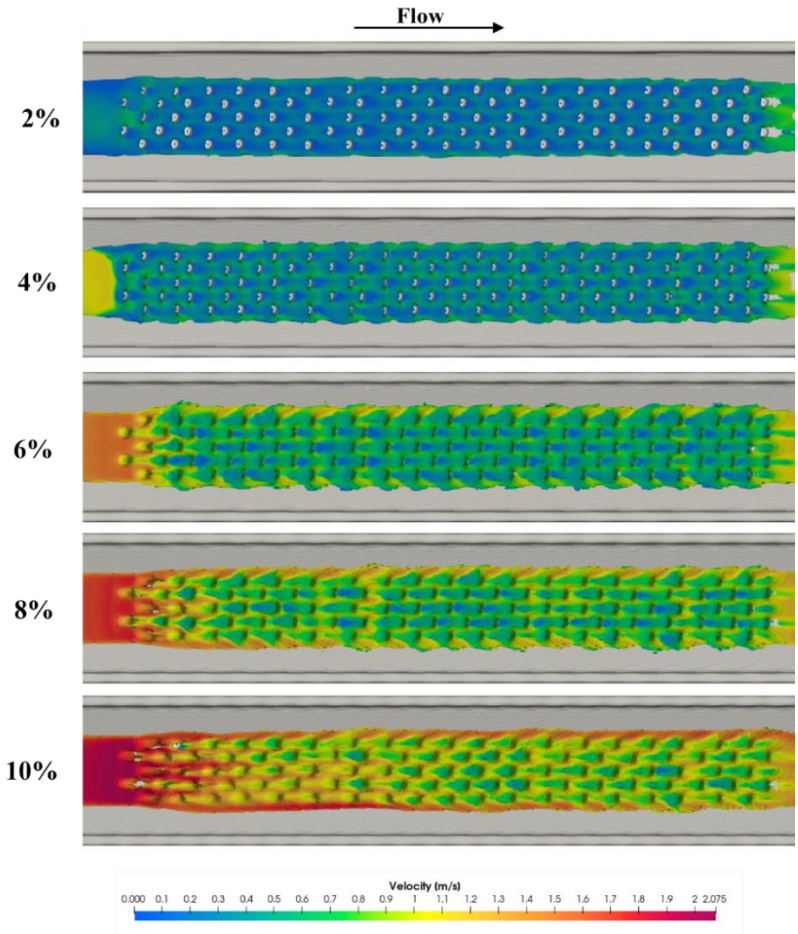


Figure 2.15: Plan view of the fishway illustrating the velocity variation for the different slopes.

Theoretically, small-bodied fish have higher chances of a successful passage in the 2% slope, as seen in Figure 2.16, because it is characterized by relatively low velocity compared to the velocities in the other slopes. Ascending the 10% slope with high velocities and turbulence can lead to high energy expenditure for the fish. This corresponds to the observation in the physical model. The maximum sprinting velocities (U_{max}) for the Arkansas Darter, the Stonecat, and the Flathead Chub are approximately 0.660 m/s (Swarr, 2018), 0.620 m/s, and 1.140 m/s (Ficke, 2015), respectively. There was high passage success for all the fish species in the 2% slope, as observed in (Swarr, 2018). This can be attributed to the U_{max} of the fish being less than the mean velocity in the 2% slope fishway. The passage success rate decreases as the slope increases. The mean velocities formed in the fishway for the 8% and 10% slopes exceed the U_{max} of all the fish species except the Flathead Chub. The low-velocity zones might have been utilized by the fish that were able to partially navigate these steep slopes. All the species could swim to an upstream distance of 4.06 m for the 10% slope but could not reach the upstream exit. Figures 2.18 to 2.21 show that the flow velocity decreases as water travels downstream. As the fish traveled upstream, the flow velocities encountered increased. The mean and maximum flow velocities in the steepest slope were 1.003 m/s and 2.075 m/s, respectively. These high velocities might have contributed to their inability to reach the upstream exit.

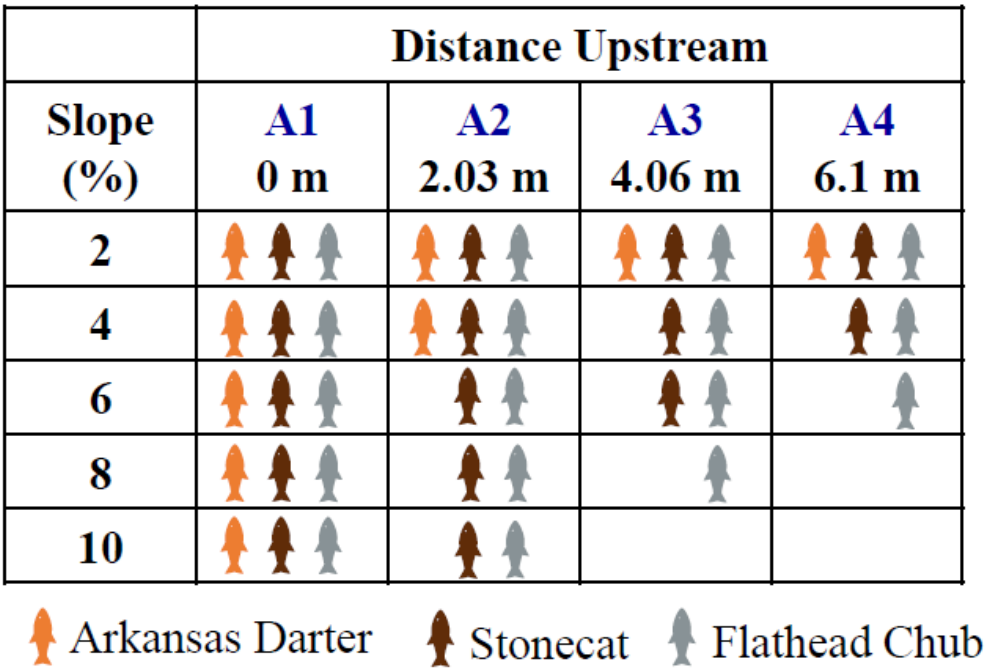


Figure 2.16: Upstream distance covered by the fish species for different slopes for passage probabilities greater than 20% (Swarr, 2018).

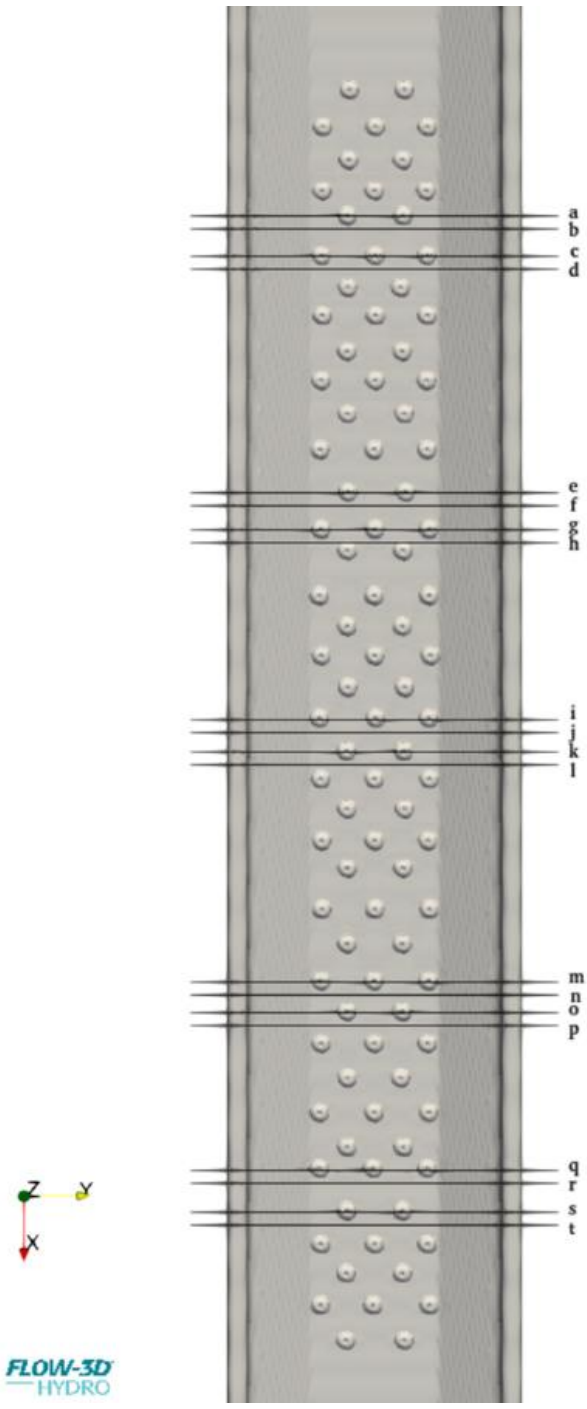


Figure 2.17: Visualized Cross-sections for the velocities between and behind the two-rock and three-rock rows. The letters represent each cross-section, where a detailed visualization of velocity is plotted in Figures 2.18 – 2.21.

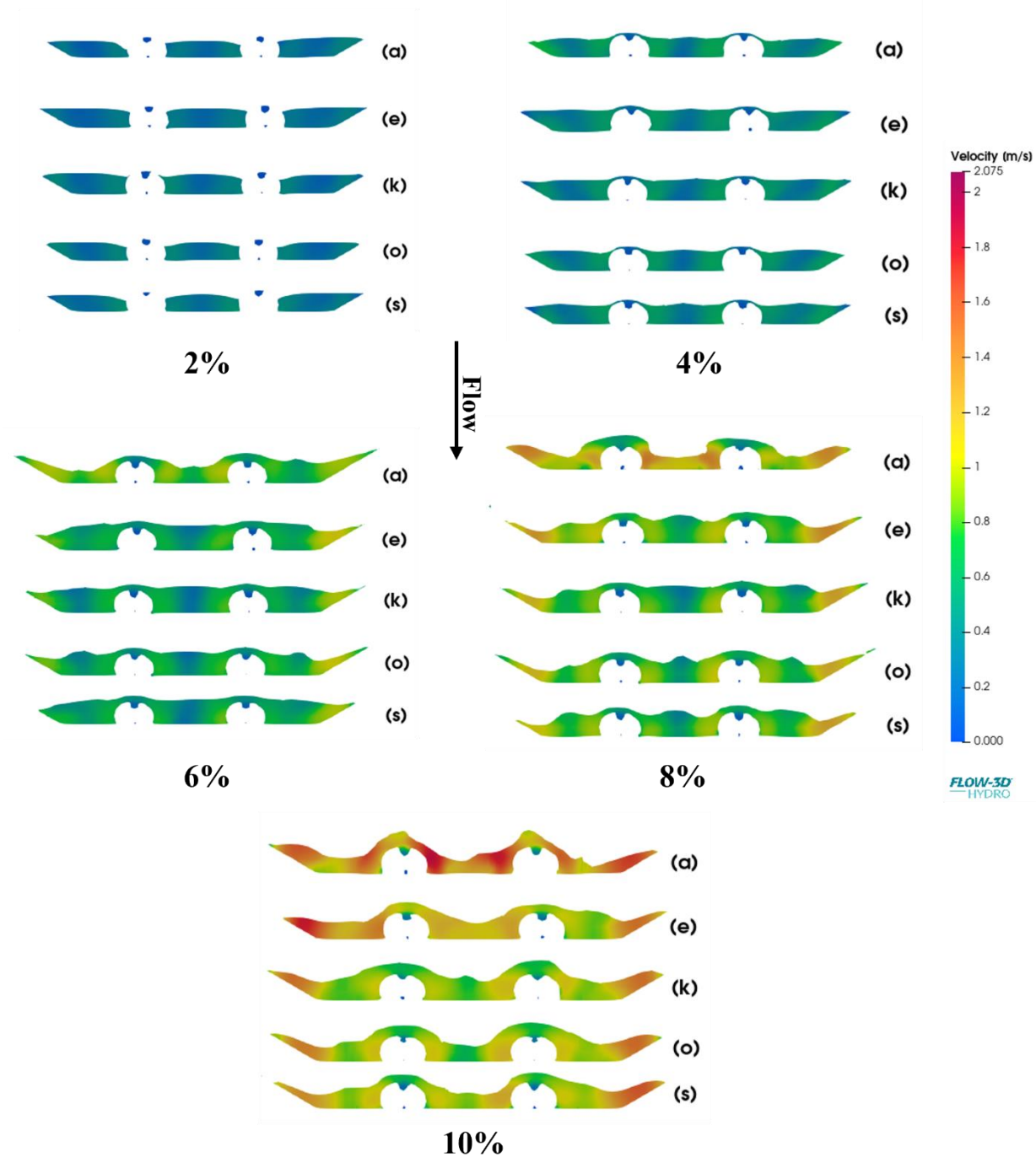


Figure 2.18: Cross-sectional velocity between two rocks.

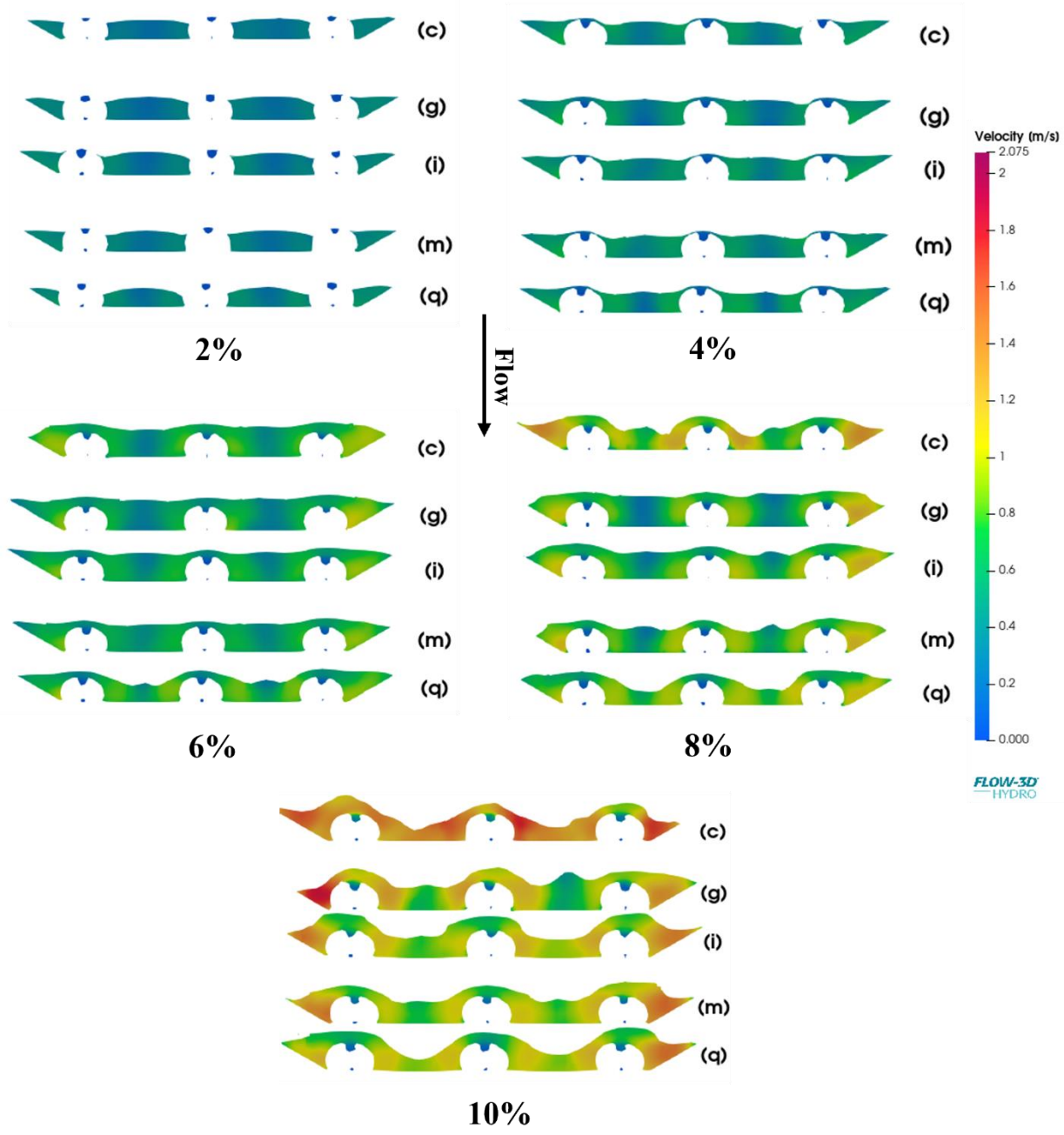


Figure 2.19: Cross-sectional velocity between three rocks.

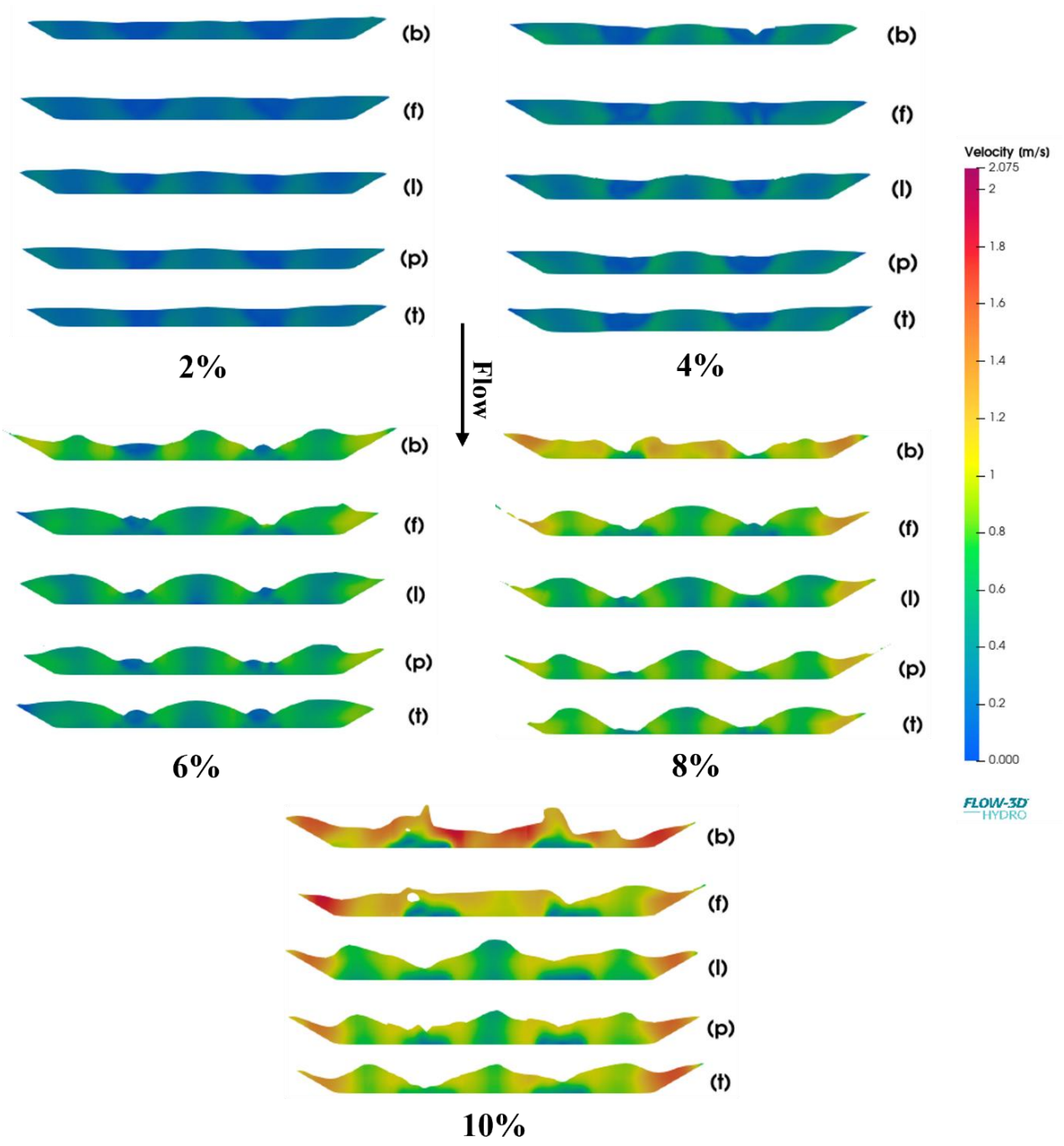


Figure 2.20: Cross-sectional velocity behind two rocks.

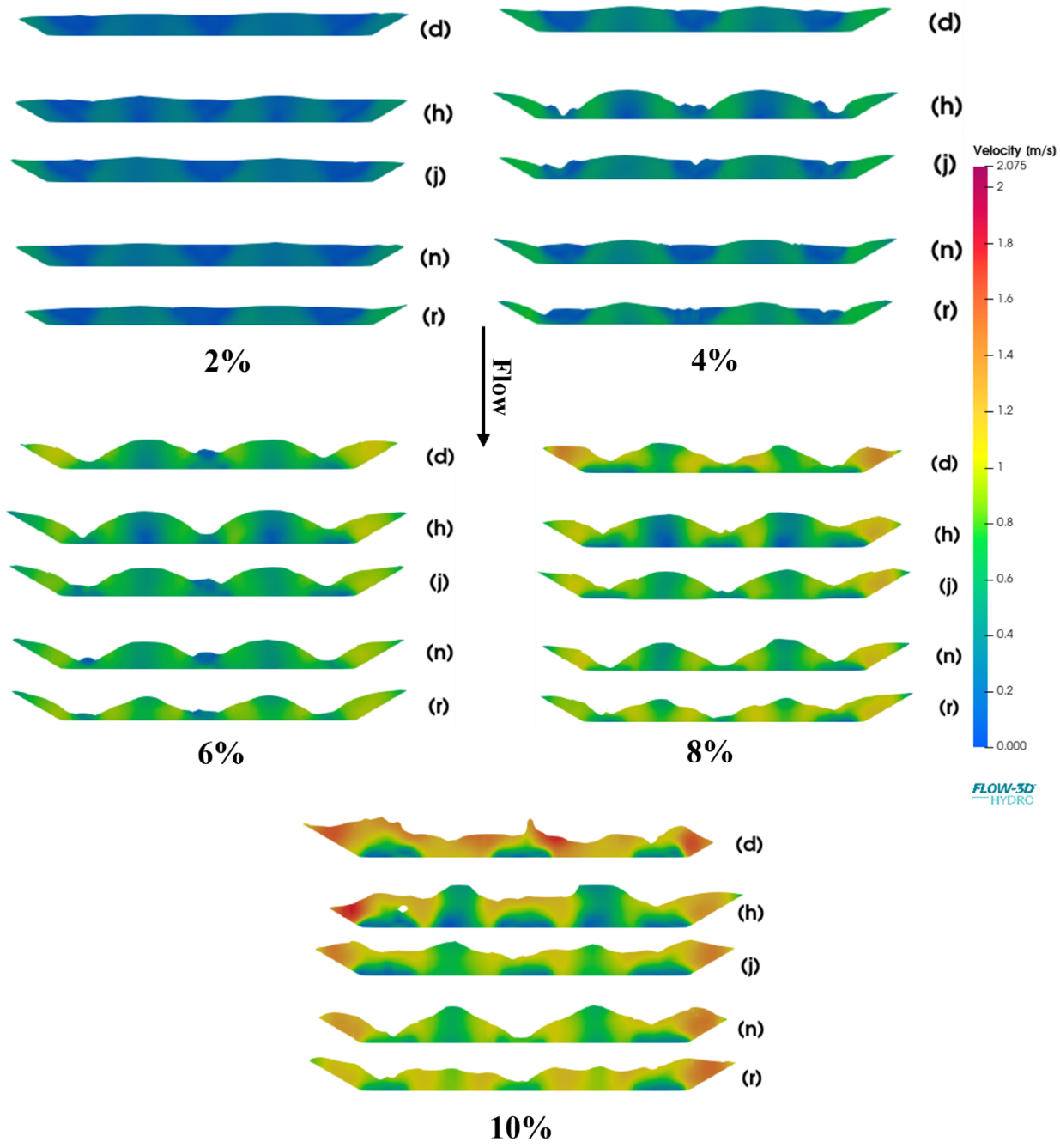


Figure 2.21: Cross-sectional velocity behind three rocks.

Turbulent Kinetic Energy

Turbulent Kinetic Energy is a measure of the average kinetic energy per unit mass of fluid in turbulent flow. In simpler terms, it is the energy of the chaos in moving water. The numerical model predictions of the TKE are illustrated in Figures 2.22 and 2.23. The mean TKE increased with increasing slopes, as seen in Table 2.8. Looking at Figure 2.22, it was observed that while most of the areas within the fishway exhibit relatively low TKE values across varying slopes, high TKE values were found at some locations. According to Table 2.8, the maximum TKE values increased with increasing slopes until reaching a peak at the 6% slope, after which there was a decline. Therefore, a maximum TKE of 0.195 J/kg was observed in the 6% slope. The fluctuation in the maximum TKE relating to slope changes can be explained by considering the dynamics of turbulence production and dissipation. At the low slope, the TKE production was low due to low velocity. As the slope increased, there was increased TKE production. However, at very high slopes, the flow became too fast that the turbulence got swept away faster than it could be generated. This phenomenon can be visualized in Figure 2.24 using the velocity vectors. More eddies were formed in the intermediate slopes compared to those of 2% and 10% slopes. The regions with higher turbulence are immediately downstream of the rocks. In this region, the flow was disturbed, and eddies were formed, contributing to higher TKE. The TKE was generally lowest near the bottom of the water column and higher near the water surface. This can be seen in Figure 2.23. The reason is that the fluid is most likely to be in contact with the solid surface of the channel bed. The solid surface can dampen the turbulence and reduce the TKE. Meanwhile, the fluid is most likely to be exposed to external forces at the surface. The TKE behavior is consistent with what was observed by Puzdrowska & Heese (2019).

Gao et al. (2016) conducted laboratory experiments in a vertical slot fishway. The researchers measured fish trajectories and used CFD software to study hydrodynamic parameters and their effect on fish movement. It was observed that fish tend to avoid areas in the fishway with TKE values above 0.35 J/kg. Instead, they prefer regions with TKE ranging from approximately 0.10 J/kg to 0.3 J/kg (Gao et al., 2016). The results of this current study show that the mean and maximum TKE values are within the favorable values for fish. Studies have shown that fish swimming performance declines when the turbulence scale exceeds two-thirds of the body length of the fish (Lupandin, 2005). The poor performance of the Arkansas Darter in the physical experiment could also be attributed to this reason. Among the three fish species studied by Swarr (2018) in the experiment, the Arkansas Darter has the smallest body length, ranging from 47 mm to 67 mm. In theory, the turbulence scale in most of the areas in the fishway at the different slopes might have exceeded the Arkansas Darter's body length. This can pose challenges for its successful fishway ascent, particularly in fishways with slopes greater than 2%.

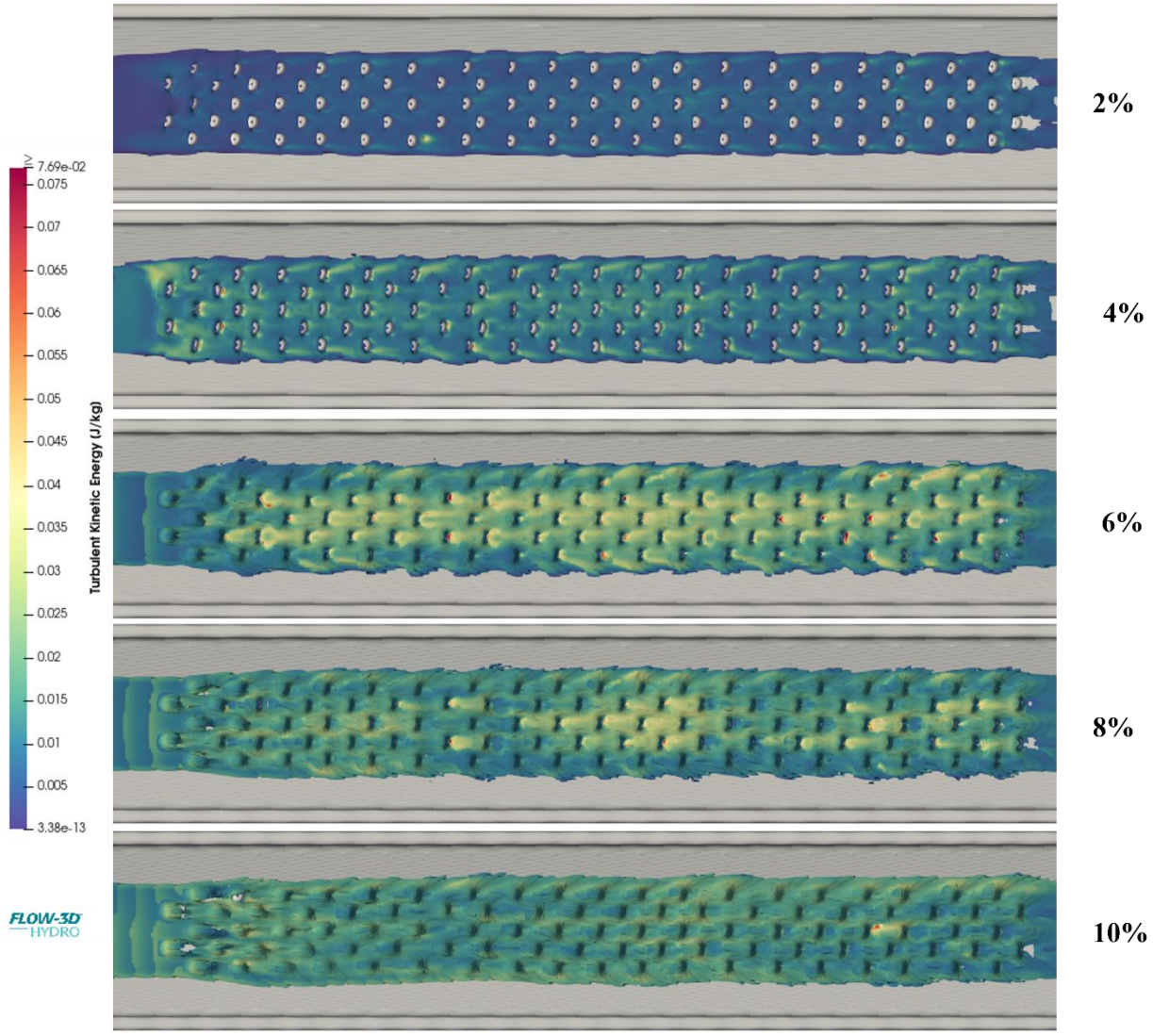


Figure 2.22: Plan view of the fishway illustrating the Turbulent Kinetic Energy for the different slopes.

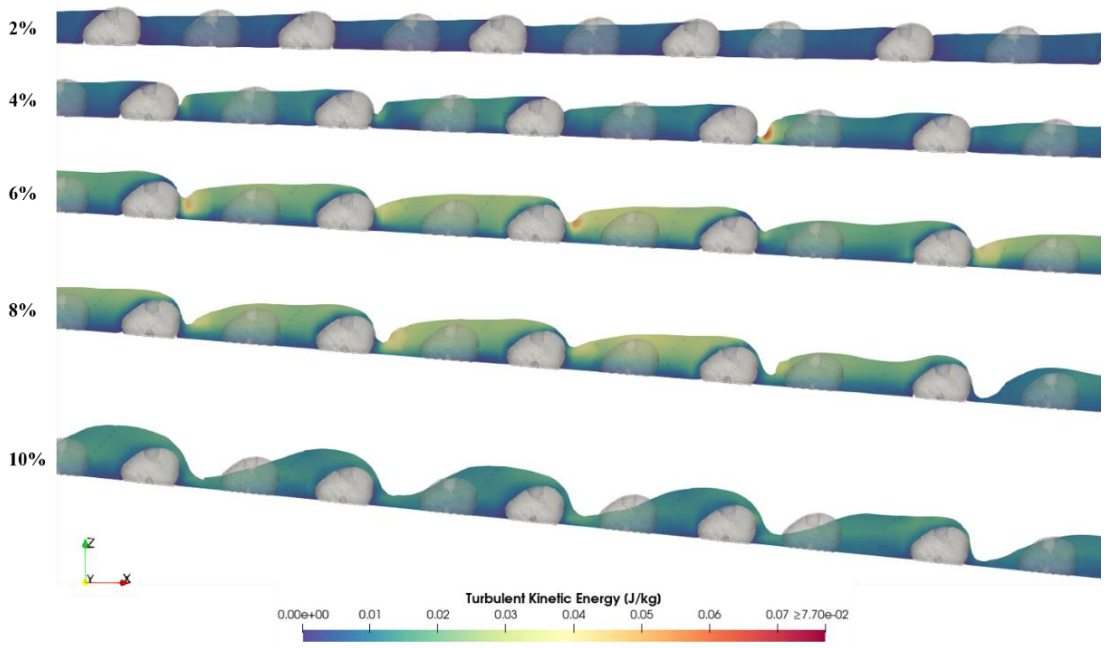


Figure 2.23: Longitudinal view of the Turbulent Kinetic Energy for the different slopes.

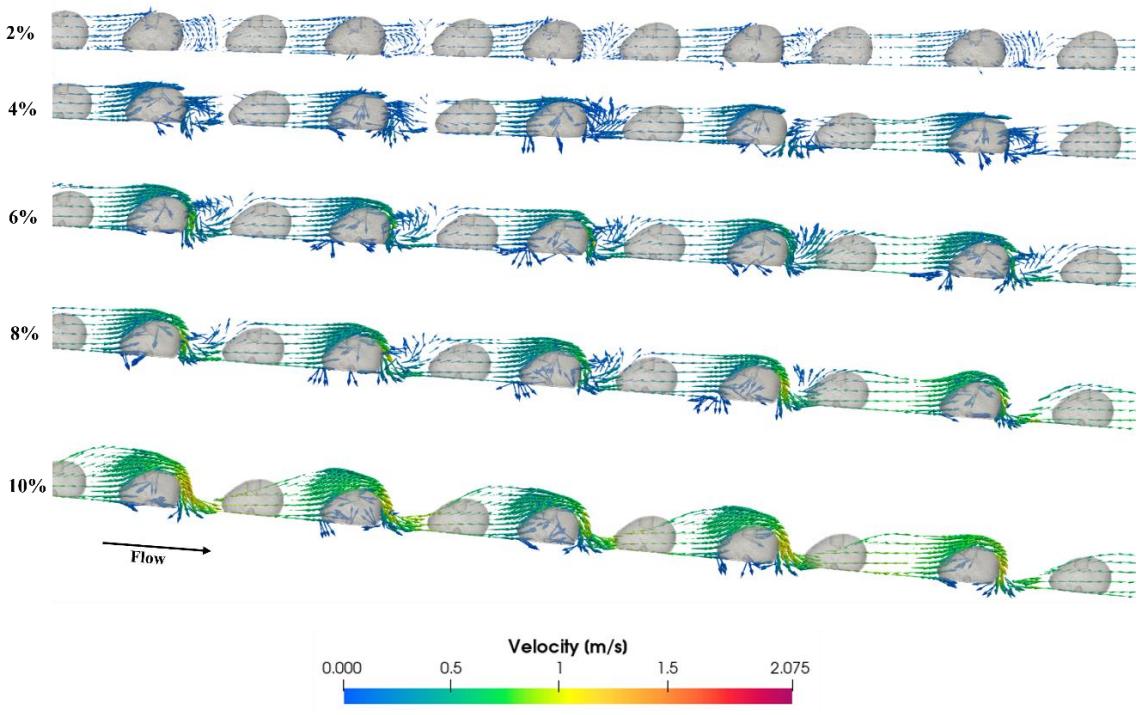


Figure 2.24: Longitudinal view of the velocity vectors for the different slopes.

Conclusion

Small-bodied fishes in the Great Plains are affected by the physical alterations in aquatic environments, such as those created by dams. There is a need to explore and improve structures such as rock ramp fishways, and their ability to provide upstream passage of fish. This study utilized CFD modeling to explore how flow characteristics, such as flow depth, velocity, and TKE, may impact small-bodied fish species. The following paragraphs highlight key conclusions from this research.

A 3D CFD software, Flow-3D Hydro, was used. The model successfully estimated flow depths and velocities. When comparing the predicted and observed flow depths for the 2% and 10% slopes, the model effectively captured water depth within the fishway, except for measurements along the longitudinal centerline of the milder slope. Similar results were also observed in the comparison of the predicted and observed velocities. Differences were only observed in the measurements taken at the longitudinal centerline for the 2% slope.

A comprehensive analysis was conducted on flow depth, velocity, and TKE within the rock ramp fishway across various slopes and flow rates using the validated CFD model. Based on the analysis, several key observations and implications emerged. The study revealed a consistent relationship between slope, flow rates, and water dynamics within the fishway. As the slope increased, the flow depths upstream of the rocks increased while they reduced downstream. The velocity also showed a proportional rise with higher slopes leading to increased flow velocities. The presence of rocks within the fishway significantly influenced flow dynamics, as expected. The rocks created distinct flow patterns, causing water to back up upstream and generating areas of low velocity in the wake region. These low-velocity zones are crucial for fish

migration, providing resting spots within fishways. The decrease in passage success rates for small-bodied fish with increasing slope observed in the physical study aligned with the higher energy expenditure required to navigate steeper inclines. The 2% slope exhibited relatively lower velocities, facilitating more successful fish passage than steeper slopes. Additionally, there is a direct relationship between the slopes and the average TKE values. The mean TKE increased with increasing slope.

The CFD modeling allowed for a detailed examination of flow depth, velocity, and TKE, offering insights that might be challenging to capture through physical experiments alone. The comprehensive nature of the study, combining experimental and numerical methodologies, contributes to a more holistic understanding of the hydraulic behavior of the rock ramp fishway. This integrated approach is essential for informing the design and optimization of fish passage structures, ensuring their effectiveness in promoting successful fish migration while considering real-world hydraulic conditions. As aquatic ecosystems face increasing anthropogenic pressures, the insights from this study serve as a valuable resource for the sustainable management and conservation of aquatic biodiversity.

Nevertheless, further research is needed to investigate the impact of rough channel beds on the flow characteristics in a rock ramp fishway by using CFD models. Additionally, there is a need to track the trajectory of the target fish species in the rock ramp fishway. By examining the movement patterns of the fish, it becomes feasible to refine our understanding of preferred fishway hydrodynamics for the target species. This will lead to a deeper understanding of the complex interactions between the small-bodied fish of the Great Plains and its hydraulic environment.

REFERENCES CITED

An, R., Li, J., Liang, R., & Tuo, Y. (2016). Three-dimensional simulation and experimental study for optimising a vertical slot fishway. Journal of Hydro-Environment Research, 12, 119–129. https://doi.org/10.1016/j.jher.2016.05.005.

Autodesk. (2023). AutoCAD (2024).

Baharvand, S., & Laskar-Ara, B. (2021). Hydraulic design criteria of the modified meander C-type fishway using the combined experimental and CFD models. Ecological Engineering, 164. https://doi.org/10.1016/j.ecoleng.2021.106207.

Baki, A. B. M., & Azimi, A. H. (2021). Hydraulics and design of fishways II: vertical-slot and rock-weir fishways. Journal of Ecohydraulics, 1–13. https://doi.org/10.1080/24705357.2021.1981780.

Baki, A. B. M., Zhu, D. Z., Harwood, A., Lewis, A., & Healey, K. (2017a). Rock-weir fishway I: flow regimes and hydraulic characteristics. Journal of Ecohydraulics, 2(2), 122–141. https://doi.org/10.1080/24705357.2017.1369182.

Baki, A. B. M., Zhu, D. Z., Harwood, A., Lewis, A., & Healey, K. (2017b). Rock-weir fishway II: design evaluation and considerations. Journal of Ecohydraulics, 2(2), 142–152. https://doi.org/10.1080/24705357.2017.1369183.

Baki, A. B. M., Zhang, W., Zhu, D. Z., & Rajaratnam, N. (2017c). Flow Structures in the Vicinity of a Submerged Boulder within a Boulder Array. Journal of Hydraulic Engineering, 143(5), 1–13. https://doi.org/10.1061/(ASCE)hy.1943-7900.0001273.

Baki, A. B. M., Zhu, D. Z., Harwood, A., Lewis, A., & Healey, K. (2020). Hydraulic design aspects of rock-weir fishways with notch for habitat connectivity. Journal of Ecohydraulics, 5(1), 94–109. https://doi.org/10.1080/24705357.2019.1652706.

Baki, A. B. M., Zhu, D. Z., & Rajaratnam, N. (2014). Mean Flow Characteristics in a Rock-Ramp-Type Fish Pass. Journal of Hydraulic Engineering, 140(2), 156–168. https://doi.org/10.1061/(ASCE)hy.1943-7900.0000816.

Baki, A. B. M., Zhu, D. Z., & Rajaratnam, N. (2015). Turbulence Characteristics in a Rock-Ramp-Type Fish Pass. Journal of Hydraulic Engineering, 141(2), 04014075. https://doi.org/10.1061/(ASCE)hy.1943-7900.0000962.

Baki, A. B. M., Zhu, D. Z., & Rajaratnam, N. (2016). Flow Simulation in a Rock-Ramp Fish Pass. Journal of Hydraulic Engineering, 142(10), 04016031. https://doi.org/10.1061/(ASCE)hy.1943-7900.0001166.

Bretón, F., Baki, A. B. M., Link, O., Zhu, D. Z., & Rajaratnam, N. (2013). Flow in nature-like fishway and its relation to fish behaviour. Canadian Journal of Civil Engineering, 40(6), 567–573. https://doi.org/10.1139/cjce-2012-0311.

Cao, H., Ye, C., Yan, X. F., Liu, X. N., & Wang, X. K. (2020). Experimental investigation of turbulent flows through a boulder array placed on a permeable bed. Water Science and Technology: Water Supply, 20(4), 1281–1293. https://doi.org/10.2166/ws.2020.046.

Carrero-Díez, L., Martínez Santa-María, C., & Fernández-Yuste, J. A. (2022). Uphill Flow Rock Ramps. How the Design Impacts Their Functionality. Water (Switzerland), 14(21). https://doi.org/10.3390/w14213492.

Cassan, L., & Laurens, P. (2016). Design of emergent and submerged rock-ramp fish passes. Knowledge and Management of Aquatic Ecosystems, 2016-January (417). https://doi.org/10.1051/kmae/2016032.

Cassan, L., Tien, T. D., Courret, D., Laurens, P., & Dartus, D. (2014). Hydraulic Resistance of Emergent Macroroughness at Large Froude Numbers: Design of Nature-Like Fishpasses. Journal of Hydraulic Engineering, 140(9), 1–9. https://doi.org/10.1061/(asce)hy.1943-7900.0000910.

Chorda, J., Cassan, L., & Laurens, P. (2019). Modeling Steep-Slope Flow across Staggered Emergent Cylinders: Application to Fish Passes. Journal of Hydraulic Engineering, 145(11). https://doi.org/10.1061/(asce)hy.1943-7900.0001630.

Cooper, A. R. (2013). Effects of dams on streams of the conterminous United States: characterizing patterns in habitat fragmentation nationally and fluvial fish response in the Midwest.

Cooper, A. R., Infante, D. M., Daniel, W. M., Wehrly, K. E., Wang, L., & Brenden, T. O. (2017). Assessment of dam effects on streams and fish assemblages of the conterminous USA. Science of the Total Environment, 586, 879–889. https://doi.org/10.1016/j.scitotenv.2017.02.067.

Dodd, J. R., Cowx, I. G., & Bolland, J. D. (2017). Efficiency of a nature-like bypass channel for restoring longitudinal connectivity for a river-resident population of brown trout. Journal of Environmental Management, 204, 318–326. https://doi.org/10.1016/j.jenvman.2017.09.004.

Duguay, J. M., Lacey, R. W. J., & Gaucher, J. (2017). A case study of a pool and weir fishway modeled with OpenFOAM and FLOW-3D. Ecological Engineering, 103, 31–42. https://doi.org/10.1016/j.ecoleng.2017.01.042.

Ficke, A. (2015). Dissertation Mitigation Measures for Battiers to Great Plains Fish Migration Submitted by Ashley D. Ficke Department of Fish, Wildlife, and Conservation Biology In partial fulfillment of the requirements For the Degree of Doctor of Philosophy Colorado.

Ficke, A. D., Myrick, C. A., & Jud, N. (2011). The swimming and jumping ability of three small great plains fishes: Implications for fishway design. Transactions of the American Fisheries Society, 140(6), 1521–1531. https://doi.org/10.1080/00028487.2011.638579

Flow Science Inc. (2023). Flow-3D Hydro (Version 2023R1).

Flow Science, Inc. (2023). Flow 3-D Hydro User Manual, Version 2023R1. Flow Science, Inc.

Franklin, A. E., Haro, A., Castro-Santos, T., & Noreika, J. (2012). Evaluation of nature-like and technical fishways for the passage of alewives at two coastal streams in New England. Transactions of the American Fisheries Society, 141(3), 624–637. https://doi.org/10.1080/00028487.2012.683469.

Fuentes-Pérez, J. F., Quaresma, A. L., Pinheiro, A., & Sanz-Ronda, F. J. (2022). OpenFOAM vs FLOW-3D: A comparative study of vertical slot fishway modelling. Ecological Engineering, 174. https://doi.org/10.1016/j.ecoleng.2021.106446.

Gao, Z., Andersson, H. I., Dai, H., Jiang, F., & Zhao, L. (2016). A new Eulerian-Lagrangian agent method to model fish paths in a vertical slot fishway. Ecological Engineering, 88, 217–225. https://doi.org/10.1016/j.ecoleng.2015.12.038.

Haro, A., Franklin, A., Castro-santos, T., & Noreika, J. (2008). Design and Evaluation of Nature-Like Fishways for Passage of Northeastern Diadromous Fishes Final Report. NOAA, 20, 1–35.

Hirt, C. W., & Nichols, B. D. (1981). Volume of Fluid (VOF) Method for the Dynamics of Free Boundaries. Journal of Computational Physics, 39, 201–225.

Hockley, F. A., Wilson, C. A. M. E., Brew, A., & Cable, J. (2014). Fish responses to flow velocity and turbulence in relation to size, sex, and parasite load. Journal of the Royal Society Interface, 11(91). https://doi.org/10.1098/rsif.2013.0814.

Juras, M., Albertson, L. K., Cahoon, J., & Johnson, E. (2018). Incorporating macroinvertebrate biological structures into gravel-bedded stream fluid dynamics using 3D CFD modelling. Ecological Engineering, 119(November 2017), 19–28. https://doi.org/10.1016/j.ecoleng.2018.05.011.

Kalathil, S. T., & Chandra, V. (2023). Experimental and numerical investigation on the hydraulic design criteria for a step-pool nature-like fishway. Progress in Physical Geography. https://doi.org/10.1177/03091333231187619.

Katopodis, C., Kells, J. A., & Acharya, M. (2001). Nature-like and conventional fishways: Alternative concepts? Canadian Water Resources Journal, 26(2), 211–232. https://doi.org/10.4296/cwrj2602211.

Katopodis, C., & Williams, J. G. (2012). The development of fish passage research in a historical context. Ecological Engineering, 48, 8–18. https://doi.org/10.1016/j.ecoleng.2011.07.004

Kirk, M. A., Maitland, B. M., Hickerson, B. T., Walters, A. W., & Rahel, F. J. (2022). Climatic drivers and ecological impacts of a rapid range expansion by non-native smallmouth bass. Biological Invasions, 24(5), 1311–1326. https://doi.org/10.1007/s10530-021-02724-z.

Koçal, Ç. (2019). Numerical modelling of free surface flows on round vertical slot fish passes. A thesis submitted to the graduate school of natural and applied sciences of middle east technical university.

Kupferschmidt, C., & Zhu, D. Z. (2017). Physical modelling of pool and weir fishways with rock weirs. River Research and Applications, 33(7), 1130–1142. https://doi.org/10.1002/rra.3157.

Lupandin, A. I. (2005). Effect of Flow Turbulence on Swimming Speed of Fish. Biology Bulletin, 461–466.

Maine Department of Transportation. (2004). Fish Passage Policy and Design Guide. March 1–22.

Mallen-Cooper, M., & Stuart, I. G. (2007). Optimising Denil fishways for passage of small and large fishes. Fisheries Management and Ecology, 14(1), 61–71. https://doi.org/10.1111/j.1365-2400.2006.00524.x.

Mao, X., Huang, S., Xu, Y., Cheng, Z., & Zhang, J. (2021). The Hydraulics of Nature-Like Fishways. Stavební Obzor - Civil Engineering Journal, 30(4), 826–834. https://doi.org/10.14311/cej.2021.04.0063.

Miranda, F. C., Cassan, L., Laurens, P., & Tran, T. D. (2021). Study of a rock-ramp fish pass with staggered emergent square obstacles. Water (Switzerland), 13(9), 1–22. https://doi.org/10.3390/w13091175.

Murry, B. A., Ania, A., Boase, J., Briggs, A. S., Chiotti, J., Fullard, C., Galarowicz, T., Hayes, D., Leonardi, J., Madel, G., & Stoller, J. (2020). Evaluation of a naturalised rock ramp fish passage for cool- and warm-water fish in a tributary of Saginaw Bay, Lake Huron. Fisheries Management and Ecology, 27(1), 77–91. https://doi.org/10.1111/fme.12392.

Özkaya, K. (2014). Numerical simulation of free surface flows at fish passages. A thesis submitted to the graduate school of natural and applied sciences of middle east technical university.

Pagliara, S., & Chiavaccini, P. (2006). Flow Resistance of Rock Chutes with Protruding Boulders. Journal of Hydraulic Engineering, 132(June), 545–552. https://doi.org/10.1061/(ASCE)0733-9429(2006)132.

Pennock, C. A. (2016). Fragmentation and fish passage: Can fishways mitigate discontinuities in Great Plains fish communities? Thesis, 2016.

Pennock, C. A., Bender, D., Hofmeier, J., Mounts, J. A., Waters, R., Weaver, V. D., & Gido, K. B. (2018). Can fishways mitigate fragmentation effects on great plains fish communities? Canadian Journal of Fisheries and Aquatic Sciences, 75(1), 121–130. https://doi.org/10.1139/cjfas-2016-0466.

Perkin, J. S., Gido, K. B., Cooper, A. R., Turner, T. F., Osborne, M. J., Johnson, E. R., Mayes, K. B., & Nilsson, C. (2015). Fragmentation and dewatering transform Great Plains stream fish communities. Ecological Monographs, 85(1), 73–92. https://doi.org/10.1890/14-0121.1.

Plymesser, K. E. (2014). Modeling Fish Passage and Energy Expenditure for American Shad in a Steeppass Fishway using a Computational Fluid Dynamics Model. PhD Thesis, January, 178.

Puzdrowska, M., & Heese, T. (2019). Turbulent Kinetic Energy in Bolt Fishway. AgriEngineering, 1(2), 265–282. https://doi.org/10.3390/agriengineering1020020.

Quaresma, A. L., Romão, F., Branco, P., Ferreira, M. T., & Pinheiro, A. N. (2018). Multi slot versus single slot pool-type fishways: A modelling approach to compare hydrodynamics. Ecological Engineering, 122, 197–206. https://doi.org/10.1016/j.ecoleng.2018.08.006.

Quaresma, A., & Pinheiro, A. N. (2014). Analysis of flows in pool-type fishways using acoustic doppler velocimetry (ADV) and computational fluid dynamics (CFD). https://www.researchgate.net/publication/307866666.

Raabe, J. K., Hightower, J. E., Ellis, T. A., & Facendola, J. J. (2019). Evaluation of Fish Passage at a Nature-Like Rock Ramp Fishway on a Large Coastal River. Transactions of the American Fisheries Society, 148(4), 798–816. https://doi.org/10.1002/tafs.10173.

Rice, W. (2021). Fish Ramps in the Inter-Mountain West and Great Plains National Fish Passage Program How Many Dams Are There? Webinar.

Richer, E. E., Fetherman, E. R., Krone, E. A., Wright, F. B., & Kondratieff, M. C. (2020). Multispecies Fish Passage Evaluation at a Rock-Ramp Fishway in a Colorado Transition Zone Stream. North American Journal of Fisheries Management, 40(6), 1510–1522. https://doi.org/10.1002/nafm.10516.

Romão, F., Quaresma, A. L., Branco, P., Santos, J. M., Amaral, S., Ferreira, M. T., Katopodis, C., & Pinheiro, A. N. (2017). Passage performance of two cyprinids with different ecological traits in a fishway with distinct vertical slot configurations. Ecological Engineering, 105, 180–188. https://doi.org/10.1016/j.ecoleng.2017.04.031.

Shiau, J., Watson, J. R., Cramp, R. L., Gordos, M. A., & Franklin, C. E. (2020). Interactions between water depth, velocity, and body size on fish swimming performance: Implications for culvert hydrodynamics. Ecological Engineering, 156. https://doi.org/10.1016/j.ecoleng.2020.105987.

Silva, A. T., Lucas, M. C., Castro-Santos, T., Katopodis, C., Baumgartner, L. J., Thiem, J. D., Aarestrup, K., Pompeu, P. S., O'Brien, G. C., Braun, D. C., Burnett, N. J., Zhu, D. Z., Fjeldstad, H. P., Forseth, T., Rajaratnam, N., Williams, J. G., & Cooke, S. J. (2018). The future of fish passage science, engineering, and practice. Fish and Fisheries, 19(2), 340–362. https://doi.org/10.1111/faf.12258.

Steffensen, S. M., Thiem, J. D., Stamplecoskie, K. M., Binder, T. R., Hatry, C., Langlois-Anderson, N., & Cooke, S. J. (2013). Biological effectiveness of an inexpensive nature-like fishway for passage of warmwater fish in a small Ontario stream. Ecology of Freshwater Fish, 22(3), 374–383. https://doi.org/10.1111/eff.12032.

Stoller, J., Hayes, D., & Murry, B. (2016). Effects of a rock-ramp fishway on summer fish assemblage in a Lake Huron tributary. Fisheries Management and Ecology, 23(5), 407–417. https://doi.org/10.1111/fme.12183.

Stuart, I. G., & Marsden, T. J. (2021). Evaluation of cone fishways to facilitate passage of small-bodied fish. Aquaculture and Fisheries, 6(2), 125–134. https://doi.org/10.1016/j.aaf.2019.02.003.

Swarr, T. (2018). Improving Rock Ramp Fishways for Small-Bodied Great Plains Fishes. Thesis. Department of Fish, Wildlife, and Conservation Biology.

Swarr, T. R., Fitzpatrick, R. M., & Myrick, C. A. (2023). Design, construction, and preliminary hydraulic evaluation of a model rock ramp fishway. North American Journal of Fisheries Management, April, 935–946. https://doi.org/10.1002/nafm.10902.

Tan, J., Tan, H., Goerig, E., Ke, S., Huang, H., Liu, Z., & Shi, X. (2021). Optimization of fishway attraction flow based on endemic fish swimming performance and hydraulics. Ecological Engineering, 170. https://doi.org/10.1016/j.ecoleng.2021.106332.

The Engineering ToolBox. (2003). Roughness & Surface Coefficients. https://www.engineeringtoolbox.com/surface-roughness-ventilation-ducts-d_209.html

Tran, T. D., Chorda, J., Laurens, P., & Cassan, L. (2016). Modelling nature-like fishway flow around unsubmerged obstacles using a 2D shallow water model. Environmental Fluid Mechanics, 16(2), 413–428. https://doi.org/10.1007/s10652-015-9430-3.

U.S. Geological Survey. (2019). Discharge measurements. https://ca.water.usgs.gov/FERC/presentations/Discharge-Measurement-Data.pdf.

Zhang, A. T., Urpelainen, J., & Schlenker, W. (2018). Power of the River: Introducing the Global Dam Tracker (Gdat). Columbia Center on Global Energy Policy, 1, 33.

Zheng, T., Niu, Z., Sun, S., Shi, J., Liu, H., & Li, G. (2020). Comparative study on the hydraulic characteristics of nature-like fishways. Water (Switzerland), 12(4). https://doi.org/10.3390/W12040955.